THESIS

PROCEDURE FOR MEASUREMENT OF SURFICIAL SOIL STRENGTH VIA BEVAMETER

Submitted by

Joseph R. Bindner

Department of Civil and Environmental Engineering

In partial fulfillment of the requirements

For the Degree of Master of Science

Colorado State University

Fort Collins, Colorado

Summer 2020

Master's Committee:

Advisor: Joseph Scalia IV
Co-Advisor: Jeffrey D. Niemann

Gregory Butters
Timothy R. Green

ABSTRACT

PROCEDURE FOR MEASUREMENT OF SURFICIAL SOIL STRENGTH VIA BEVAMETER

Spatial prediction of moisture-variable soil strength is critical for forecasting the trafficability of vehicles across terrain. The Strength of Surface Soils (STRESS) model calculates soil strength properties as a function of soil texture from SSURGO data (or locally available data) and soil moisture from the Equilibrium Moisture from Topography, Vegetation, and Soil (EMT+VS) model. The STRESS model yields soil strength properties (friction angle and moisture-variable cohesion) that vary with soil texture and moisture conditions. However, the STRESS model is hindered by a lack of surficial soil strength data linked directly to soil texture. The objective of this study is to develop and validate a bevameter procedure to improve measurement of near-surface moisture-variable soil strength. The bevameter is a test apparatus that measures in-situ surficial soil strength properties by rotational shearing of a shear annulus under a constant normal force at a constant rate. The bevameter allows for lab or field determination of Mohr-Coulomb surficial soil strength properties at a given moisture content in a manner that approximates how vehicles interact with surficial soils. Experimental variables evaluated include the shearing surface (grousers, sandpaper, or bonded angular sand) and the use of interior and exterior annular surcharge weights to minimize slip sinkage of the shear annulus. Based on the results of this study, a bevameter procedure is recommended that uses a coarse sandpaper as the shear interface with an internal and external surcharge of 2 kPa during shear testing. Using the revised bevameter procedure for field testing, the performance of predicted

moisture-variable soil strength by the STRESS model is evaluated. Field validation illustrates the need to develop surficial-soil specific pedotransfer functions for use in the STRESS model.

ACKNOWLEDGEMENTS

This research was made possible by the generous support of the U.S. Army Research Laboratory (ARL) and the Leonard Wood Institute (LWI). I would like to thank Dr. Joseph Scalia and Dr. Jeffrey D. Niemann for their continual guidance and support on this project and committee members Greg Butters and Tim Green for their collaboration on the project. I would like to thank Matt Pauly for his significant contributions to the project and Thomas Mayer for his great assistance in the lab.

TABLE OF CONTENTS

1. INTRODUCTION

Agriculture, construction, mining, logging, and military operations rely on an understanding of vehicle mobility on off-road terrain (Wong, 2001). Remote prediction of vehicle mobility is critical because field determination of vehicle mobility may not be practical for many applications. Terramechanics is the study of soil behavior relevant to off-road vehicle performance and is of particular interest to army and peace keeping operations around the world. The North Atlantic Treaty Organization (NATO) Reference Mobility Model (NRMM) was developed by the U.S. Army Tank Automotive Research, Development, and Engineering Center (TARDEC) and the Engineer Research and Development Center (ERDC). The NRMM was developed as a vehicle mobility simulation tool in the 1960s and has continually been used and revised in the decades since (Balling et al., 2019). The NRMM considers a vehicle's maximum mobility potential based on terrain, vehicle, and operator variables (Lessem et al., 1996). The trafficability of off-road terrain is analyzed by considering soil texture, soil moisture, soil strength, slope, surface roughness, and obstacles, among other characteristics.

Predicting accurate soil strength is critical for mobility models such as the NRMM. While surficial soil strength is primarily controlled by soil texture (percent sand, silt, and clay), soil moisture and density are also important. The soil strength input to the NRMM is empirically derived from a cone penetrometer. During cone penetrometer testing, a small cone is pressed into the surficial soil layers at a contestant rate. The force applied to the cone is divided by the cone area and reported as a dimensionless parameter termed cone index (CI). For fine grained soils, the procedure is repeated on a remolded sample, with the ratio of the remolded CI to the original CI referred to as the remolding index (RI). The RI can be multiplied by CI to produce a soil strength

parameter termed rating cone index (RCI). For coarse grained soils, RCI and CI are the same value (RI = 1). The measured RCI is then related to the mobility of a given vehicle at a specific speed on the same soil under the same conditions. The RCI has been the preferred method for measuring in-situ soil strength for vehicle mobility because of the simplicity and low cost of the method (Shoop, 1993). However, RCI cannot be easily adjusted for variable levels of soil moisture or for forecasting mobility of untested vehicles (e.g., using increasingly common computer simulations to optimize designs).

The Strength of Surface Soils (STRESS) model (Pauly, 2019) can be used to produce fine resolution estimates of moisture-variable soil strength when paired with the Equilibrium Moisture from Topography, Vegetation, and Soil (EMT+VS) model. The EMT+VS model conducts a water balance on the hydraulically active soil layer to generate fine resolution patterns of soil moisture (Ranney et al., 2015). The STRESS model applies unsaturated soil mechanics using soil moisture inputs from the EMT+VS model and available soil texture data. As a soil becomes unsaturated, a negative pore water pressure develops, referred to as suction stress (Bishop and Blight, 1963; Fredlund et al., 1978; Lu and Likos, 2004; Lu et al., 2010). Suction stress contributes to soil strength and is unique for a given soil at a given water content. The STRESS model uses binned soil strength parameters based on Unified Soil Classification System (USCS) class average strength parameters to estimate surficial soil strength for vehicle mobility. However, the performance of the STRESS model is limited by existing class average soil strength datasets (Pauly, 2019). Thus, a need exists to collect surficial soil strength parameters tied to soil texture to improve remote prediction of soil strength. Methods to measure surficial strength are also needed to validate such models and understand spatial variability and uncertainty in predicted soil strengths.

The Bekker Value Meter (Bevameter) was developed to measure surficial soil strength under conditions similar to those produced by mobilized vehicles (Bekker, 1969). The device measures in-situ surficial soil strength by rotational shear. Although the bevameter has been studied for over fifty years, bevameter data are sparse and a consistent procedure has not been established.

The objective of this study is to develop a bevameter testing procedure for the future development of a terramechanics-focused soil strength database. Bevameter procedural variables were tested and a method is proposed in Chapter 2 that reduces current uncertainties in soil strength measured by bevameter (Bevameter Procedure Development). Soil strength parameters generated by bevameter using the revised procedure are then compared to direct shear and triaxial test results on the same soil. Next, a series of field tests are described that were conducted using the revised bevameter procedure (Chapter 2) and are used to explore the predictive capability of the STRESS model in Chapter 3 (STRESS Model Evaluation).

2. BEVAMETER PROCEDURE DEVELOPMENT

1. Introduction

Measuring shear resistance of surface soils is critical to validate models that predict vehicle mobility across terrain (Bekker, 1956). Surficial soil strength can be measured ex-situ or in-situ. Ex-situ methods require collecting samples, transporting samples back to a lab, then testing the soil. Collecting, transporting, and preparing ex-situ samples for tests such as the triaxial and direct shear test results in sample disturbance. In-situ methods are preferred because they minimize sample disturbance (Wong, 2001). For terramechanics applications, in-situ soil strength tests are performed by devices such as the cone penetrometer or bevameter.

Two soil strength parameters of interest to describe soil strength are friction angle (ϕ) and cohesion (c). Friction angle is a material property that depends on soil texture while c varies with both soil texture and soil moisture. Effective c is characterized by soil strength contributions from electrostatic forces between soil particles that vary with soil texture (percentage of sand, silt and clay) and fabric. Apparent c is the strength contribution from negative pore water pressure (suction stress) which develops in unsaturated soil. The STRESS model combines effective and apparent c to produce a parameter termed moisture-variable cohesion (c_θ) which is measured by a bevameter (Pauly, 2019).

Geotechnical engineering has incorporated c and ϕ in civil engineering earthwork since Coulomb in 1776 (Osman, 1964). However, these parameters did not make an introduction to the study of terramechanics until the 1960s. Terramechanics studies have shown that soil resisting forces to vehicle thrust are dependent on c, ϕ, and density (Payne, 1956). Therefore, the accurate

measurement of ϕ and c is critical for the analysis of vehicle mobility across terrain (density is not the focus of this study; Osman, 1964).

While there are many methods which can be used to measure in-situ soil strength that still allow direct calculation of strength parameters; the bevameter has been argued to be the most representative of soil-vehicle conditions that provides direct measurement of physics-based soil strength parameters (Wong, 2001; Oravec, 2009; Edwards et al., 2017). Although the bevameter has been studied for over 50 years, comprehensive bevameter data are scarce, and the device lacks a standardized procedure for collection of shear strength parameters. While the bevameter rotational shear test has been shown to generate reproducible results, the device has known limitations which have not been quantified (Pauly, 2019) or addressed. As a result, the reliability of the limited data is unknown.

A phenomenon referred to as slip sinkage is a leading concern for bevameter testing. Slip sinkage refers to the sinkage of an object through the action of shearing with a loaded mechanism (Liston, 1973). To accurately determine shear stress acting on a soil, the area of the failure plane must be known. In bevameter testing, an imbalance of forces causes a failure plane to develop oblique to the shearing surface, making the area and forces acting on the failure plane impossible to accurately calculate, leading to inherently inaccurate strength measurement (Liston, 1973). To mitigate the influence of slip sinkage, Nowatzki and Karafiath (1972) suggested placing weighted annular plates around the shear annulus, but no recommendations were made as to the magnitude or orientation of the surcharge. Janosi and Karafiath (1981) conducted a study to measure the external annular surcharge to a bevameter required for adequate reduction of shear annulus sinkage. However, annular plate surcharge recommendations were only given for external

surcharges and only for grousers as the shear interface which deepen the interface and necessitate heavy plates for surcharge that are largely impractical for field testing.

The objective of this study is to develop a field-deployable method for soil strength testing by bevameter to measure surficial soil strength. In efforts to eliminate the development of an oblique failure plane in bevameter testing, this study explores how altering several bevameter method variables affects the magnitude of shear annulus slip sinkage and alters the generation of surficial soil strength parameters. A human-powered bevameter shear strength device is used to explore slip-sinkage. This bevameter was designed for efficiency in field testing by reducing the machine size, weight, and power requirements. The device uses dead weight to provide an annular normal force and human power to induce shear stress in the soil. Various shear interfaces, surcharge plate locations, and surcharge magnitudes, are tested to develop a procedure for bevameter testing that is readily field deployable.

2. Background

When measuring soil strength for vehicle mobility applications, generating parameters that accurately reflect forces and failure modes present under vehicles is critical (Bekker, 1969; Okello, 1991; Wong, 2001). Many devices have been proposed to measure ϕ and c of in-situ soils, yet there are limited data comparing the results between devices and against existing methods used by geotechnical engineers. Several of the shear strength devices have been argued to generate stress orientations and failure modes that are not representative of those developed by a wheeled or tracked vehicle (Wong, 2001; Edwards et al., 2017). Numerous studies have suggested that the most suitable tests for vehicle mobility are those that simulate the ground contact area of a wheel or track and apply stresses to the soil similar to that of a vehicle (Bekker, 1969; Wong, 2001; Edwards et al., 2017). The terramechanics literature generally recommends the bevameter as the

preferred method for soil strength measurement (Okello, 1991; Wong, 2001; Oravec, 2009; Edwards et al., 2017; Mason et al., 2019).

Studies conducted to better understand soil failure beneath a wheeled vehicle suggest shear soil stress acts parallel to the radial plane of the wheel (Nowatzki and Karafiath, 1974; Moreland et al., 2011). Figure 2.1 and 2.2 display how failure occurs beneath the bevameter shear annulus and underneath a vehicle wheel. Soil failure beneath a vehicle develops from a thrust parallel to the soil surface provided by a vertically loaded wheel or track. Similarly, the bevameter generates a force parallel to the soil surface under a vertical normal load, producing shear conditions similar to those produced by vehicles.

In contrast to how shearing resistance is mobilized by a bevameter during shear strength testing, shearing resistance in triaxial testing used by geotechnical engineers is inferred from the axial deviator stress which is increased until the specimen fails. Triaxial failure is expected to follow a Rankin passive failure mode, with shear stresses developing at an angle of $45° + \phi/2$ to the horizontal plane as shown in Figure 2.3 (Edwards et al., 2017). Triaxial testing holds the advantage of allowing testing at higher stresses without the need for large equipment or loads. Higher shear strengths are typically observed in ex-situ testing (e.g., triaxial) than in-situ (e.g., bevameter) due to the natural heterogeneity of soils (Bowles, 1992), and the differences that different failure planes make on realized soil shear strength during testing; although, this observation is not universal.

3.2.1 Bevameter

The bevameter is a device used to conduct two in-situ tests. The bevameter can be used to conduct a pressure-sinkage test to determine the compressive characteristics of the soil and a

rotational shear test to generate shear-strength parameters. The pressure-sinkage test is not the focus of this study. The rotational shear test is conducted by shearing the soil via an annular plate by applied torque at a constant rate to determine the shear strength of the soil. A shear annulus is placed on the soil and loaded with a force normal to the soil surface that is provided by dead weight or a mechanical system with sufficient reactive mass. The shear annulus is rotated at a constant rate while recording the torque required to rotate. This test is conducted using at least three different normal loads to generate a Mohr-Coulomb failure envelope to calculate shear strength parameters. Relevant normal stresses for testing were analyzed in a literature review by Pauly (2019) and the normal stresses of 19.2 kPa, 38.6 kPa, and 58.7 kPa were identified as being relevant to vehicle mobility and are adopted herein for bevameter testing.

From the bevameter tests, data are used to generate plots of shear stress versus shear displacement referred to as shear-deformation curves. Example peak shear strengths are shown on shear deformation curves in Figure 2.4. For each test, the peak shear stress is plotted against the normal stress and a line is fit to the data using the method of least squares liner regression to determine c and ϕ. Peak shear stress is typically defined where shear strength alters from strain-hardening to strain-softening. However, in some soils, sinkage of the shear annulus leads to increased shear strength with depth, in which case peak shear strength is reported as the strength at which the slope of the shear deformation curve drastically changes.

The goal of the bevameter shear interface is to measure soil strength by ensuring soil failure occurs between soil particles within the tested soil and not between the tested soil and shear interface. Various shear interfaces have been used in rotational shear testing including grousers, rubber, and sandpaper. However, these shear interfaces have not been researched comparatively regarding the impact of the interface type on slip sinkage and measured shear strength parameters.

Arguments have been made that grousers help ensure that failure occurs between soil particles and not between the soil and shearing interface. However, as shown schematically in Figure 2.6, soil flow behind grousers may occur in loose soils leading to inaccurate measurement of soil strength (Reece, 1964). Finally, the lab sample size required for accurate testing of soils by bevameter has not been explored.

3.2.2 Triaxial Testing

Figure 2.7 shows a typical in lab triaxial test setup used to determine soil shear strength parameters under controlled drainage conditions. Cylindrical soil specimens are either prepared in a laboratory from bulk soils or collected as intact field samples. Specimens are encased in an impermeable latex membrane with a porous stone on either side to promote drainage. The specimen is placed in a pressure cell and tubes attached to the specimen are connected to a pressure panel. The pressure cell is inundated with water and specimen cell and pore water pressures are controlled by the pressure panel. The specimen is then consolidated to the desired effective confining stress and placed in a shearing apparatus that axially loads the specimen at a constant strain rate. The specimen in typically sheared to 15 to 20% strain before the test is terminated.

Triaxial testing is commonly used for traditional geotechnical applications. For example, the triaxial test is often used for analyzing soil strength in earthen structures (e.g., embankment dams) and beneath proposed structures. However, triaxial testing is time consuming, expensive, and complicated. In addition, because triaxial testing is an ex-situ method, arguments have been made that the triaxial test does not accurately represent vehicle stress conditions for determination of vehicle soil strength properties (Wong, 2001). Additionally, samples must be collected and

transported to a lab from an off-site location were the sample is then further handled for specimen preparation, increasing the likelihood of sample disturbance.

3.2.3 Direct Shear

The direct shear test is used to determine the shear strength of a soil specimen in the laboratory (ASTM D 3080/D 3080M-11, 2011). Soil is prepared in a shear box that has two halves that are locked together during preparation (Figure 2.8). Porous stones are placed in the shear box on either end of the specimen to promote drainage. The shear box is then placed in the direct shear device and the two halves of the shear box are unlocked. A piston is placed on top of the shear box and a normal force is applied via the piston, imparting a normal stress on a predetermined failure plane. Shear stress is induced by applying a constant rate of displacement to half of the box while keeping the other half in place. As the soil is sheared, the force required to displace the box half is recorded. The test is repeated for at least three different normal stresses. The peak shear stress for each test is plotted against the respective vertical normal stress. A Mohr-Coulomb strength envelope can be fit to the data for determination of ϕ and c.

The direct shear test is less difficult to prepare and takes less time to run than a triaxial test. However, values for ϕ are generally overpredicted in sands relative to the triaxial test (Bowles, 1992). This overprediction is attributed to forcing the location of the failure plane instead of allowing the soil to fail along the weakest plane. Samples are also small which may amplify the effects of heterogeneity in the soil (Bowles, 1992). In addition, the direct shear test is a laboratory test and sample stresses do not replicate in-situ conditions. Arguments have been made that the direct shear test does not accurately represent soil strength for vehicle mobility applications (Okello, 1991; Wong, 2001; Senatore and Iagnemma, 2011).

3.2.4 Cone Penetrometer

The Waterways Experiment Station (WES) of the U.S. Army Corps of Engineers developed the cone penetrometer as a convenient empirical tool to quantify the trafficability of soils (Figure 2.9). The device measured the combined effect of soil drag and soil thrust relevant to vehicles into a single value (Bekker, 1969). The cone penetrometer measures the force required to advance a 645 mm^2 (1 square inch) cone into the soil at a rate of 30.5 mm/second (1 inch/second; Humboldt, 2011). The force measured is defined as the cone index (CI). Measurements are taken every 76 mm to a depth of 457 mm (Humboldt, 2011). The test is conducted five to seven times to generate an average CI (Shoop, 1993). In the case of fine-grained soils, the remolding index (RI) is also measured. A soil sample is remolded by imparting 100 blows with a 1.14-kg cylinder from a height of 300 mm (Shoop, 1993). For sands containing fines, 25 blows are imparted on the soil sample. The cone index is then measured on the remodeled soil. Remolding index is calculated by taking the ratio of the remolded CI to the in-situ CI (Stevens et al., 2013). The rating cone index (RCI) is then calculated by taking the product of the CI and RI. Rating cone index can be related to the trafficability of a given vehicle through the vehicle cone index (VCI) which represents the minimum RCI required for a specific vehicle to consistently make a specified number of passes at a certain speed (Stevens et al., 2013).

While the cone penetrometer offers low cost soil data that is easy and quick to generate, the test has substantial limitations. The test can be used to predict trafficability for existing vehicles which have been physically tested; however, the empirical correlation cannot be easily extended to in-design or untested vehicles. The cone penetrometer produces a single index which cannot replace the shear strength parameters, ϕ and c, used to define shear strength for physics based models (Janosi and Karafiath, 1981). In addition, because soil strength is a function of soil

moisture, adjusting RCI for changes in moisture content is difficult because the RCI does not differentiate between strength contributions from apparent and effective soil strength.

3. Methods and Materials

3.3.1 Silty Sand

A silty sand was used for testing (USCS SM). Sieve analysis, hydrometer, Atterberg limits, and specific gravity were used to characterize the soil. Results of these tests are summarized in Table 2.1.

3.3.2 High Plasticity Clay

A high plasticity clay (USCS CH) was used for soil testing and classification. Results from characterization tests are summarized in Table 2.1. Standard proctor tests were conducted at nine different gravimetric water contents ranging from 13% to 28%. A third-order polynomial function was fit to the data using the method of least squares. The optimum water content was calculated by taking the first derivative of the polynomial equation and solving the resulting quadratic equation. Maximum dry density was then solved by inputting the optimum water content into the original polynomial function. Samples were compacted in a split, 102 mm, standard Proctor mold using a manual compaction hammer.

3.3.3 Poorly Graded Sand

A ground silica sand (USCS SP) was used for testing (W.W. Grainger Inc., Lake Forest, IL). Sieve analysis was conducted on the sand for classification. Results are summarized in Table 2.1

3.3.4 Bevameter Testing

A human powered bevameter was used for shear strength measurement. The bevameter had a shear annulus with a 10 cm inner diameter and 15 cm outer diameter. Three tests were conducted under different normal stresses (19.2 kPa to 58.7 kPa) to develop Mohr-Coulomb parameters. The shear annulus was rotated at 1 rpm for 360 degrees to measure peak and residual strength; 1 rpm results in an outer-edge velocity of 471 mm/minute, an inner-edge velocity of 314 mm/minute, and a velocity at the annulus midpoint of 393 mm/minute. During rotation, torque was measured using an Interface TS12 Shaft Style Reaction Torque Transducer (Interface Inc., Scottsdale, AZ, USA) mounted on the shaft by an Inch-Metric Conversion Coupling (Stafford Manufacturing Corp., Wilmington, MA). As shown in Figure 2.10, sinkage was measured by a HM-740, 5 cm Linear Variable Displacement Transducer (LVDT; Gilson Company Inc., Lewis Center, OH, USA) attached to the bevameter frame with the end of the sensor resting on the top of the shear annulus. The spring loaded LVDT core extension could freely move up and down with the shear annuls as the annulus was rotated. Torque and displacement sensor outputs were processed and recorded using LabVIEW (National Instruments, Austin, TX, USA). Data were recorded on a laptop computer.

The first stress applied to the shear annulus corresponds to the weight of the shear annulus, torque sensor, shear shaft, and moment arm, resulting in a normal stress of 19.2 kPa. The second normal stress was achieved by adding a 20.4 kg iron weight to the shear shaft, resulting in a normal stress of 38.6 kPa (Figure 2.11). The third normal stress was achieved by adding an additional 20.4 kg plate weight atop the first weight resulting in a normal stress of 58.7 kPa. These stresses were selected based on literature to produce shear stresses in soil for generation of surficial soil strength parameters.

Bevameter shear testing was conducted in a galvanized steel tank with a diameter of 90 cm and a height of 58 cm with the bevameter placed in the middle of the tank atop the soil. Soil was prepared at a relative density of 85% of standard Proctor maximum dry density to represent in-situ soil density (Pauly, 2019). The soil was prepared to a thickness of 15 cm to ensure failure plane did not extend to the soil-container interface. Bevameter legs were fastened using 6 Hand Brakes for Sleeve Bearing Carriage for T-Slotted Framing (McMaster-Carr, Aurora, OH).

Equation 1, proposed by Janosi and Hanamoto (1961), was used to convert torque into shear stress (τ) for rotational shear testing.

$$\tau = \frac{3T_m}{2\pi(r_o^3 - r_i^3)} \tag{1}$$

where T_m is the torque developed in the shaft attached to the shear annulus, r_i is the inner radius of the shear annulus and r_o is the outer radius of the shear annulus, assuming no friction between the shaft and bearings. A trend line was fit to each peak shear stress versus normal stress plot using least squares regression to represent the Mohr-Coulomb failure envelope. The ϕ was calculated by taking the inverse tangent of the failure envelope slope and c was represented by the shear strength intercept.

3.3.5 Shear Interface Testing

A series of tests were conducted to evaluate the effects of varying shear interface materials on measured soil strength. Three interfaces were tested using shear annuli. The three shear interfaces tested are shown in Figure 2.12. The first shear interface tested consisted of 12 evenly spaced metal grousers fixed to the shearing ring (Figure 2.12a). Each grouser extended 16 mm

perpendicular to the surface of the shear annulus, and had a width of 25.4 mm. The second shear interface tested was a coarse angular sand bonded to the bottom of a shear annulus by a high-strength epoxy (Figure 2.12b). The third shear interface tested was an adhesive-backed sandpaper (40 grit; Ace Hardware Brand) cut to the dimensions of the shear annulus (Figure 2.12c). All shear interfaces were tested on air-dried SM with no internal or external surcharge.

3.3.6 Surcharge Location Testing

The three shear interfaces described in Section 3.3.5 were tested under three different surcharge plate conditions: no surcharge, external surcharge plate, and an internal and external surcharge plate. The positions of internal and external surcharge plates are shown in Figure 2.13. These surcharge conditions were tested to evaluate the impact of surcharge on the magnitude of slip-sinkage. The internal surcharge was provided by low-carbon steel discs with a diameter of 89 mm and height of 25 mm, weighing 1.28 kg and providing a 2 kPa surcharge per disc. Three discs could be stacked within the shear annulus before exceeding the internal height of the annulus. External surcharge was provided by placing weights on a 13 mm thick HDPE plastic ring with inner diameter of 165 mm and outer diameter of 216 mm (Figure 2.14). All surcharge presence and location evaluation tests were conducted under a 6 kPa surcharge for consistency.

3.3.7 Surcharge Magnitude Testing

Seven combinations of internal and external surcharge, listed in Table 2.5, were tested to evaluate the effect of surcharge magnitude on shear annulus sinkage. A shear annulus normal stress of 58.7 kPa was chosen to replicate the maximum load used for field testing. Testing was conducted in two series. Testing Series 1 used internal surcharges of 2 kPa, 4 kPa, and 6 kPa and

external surcharges of 2.6 kPa, 5.6 kPa, and 8.7 kPa, respectively. Testing Series 2 used the same internal surcharges as Testing Series 1 with external surcharges matching the stresses produced by the internal surcharge (2 kPa, 4 kPa, and 6 kPa). All surcharge conditions were repeated a minimum of four times (additional tests were performed at select combinations to evaluate reproducibility, described subsequently).

3.3.8 Sinkage-Measurement Reproducibility Testing

To evaluate the reproducibility of sinkage magnitude measurements, two testing conditions were selected for additional replication. An internal surcharge of 2 kPa and external surcharge of 2.6 kPa was used to evaluate the reproducibility of sinkage measurements by conducting eleven replicate tests. Eight additional tests were conducted with a paired internal and external surcharge of 2 kPa to further evaluate reproducibility.

3.3.9 Shear Zone Testing

Bevameter testing was conducted to evaluate the depth of the shear zone. Sandpaper was used as the shearing surface with an internal and external surcharge of 2 kPa. A rectangular mold was used to place a fine black sand into the SM (Rolf C. Hagen Corp., Mansfield, MA). Figure 2.15 illustrates the two sands placed side by side for comparison. The mold had a height of 100 mm, length of 200 mm, and width of 25 mm. During compaction, the mold was placed on the surface of the SM and the exterior was filled with SM until approximately 20 mm of the mold remained exposed above the surface of the silty sand. The mold was then filled with the fine black sand until the two soils were level. Finally, the mold was slowly removed. The SM and fine black sand were compacted to 85% standard Proctor maximum dry density. The shear annulus was

centered atop one end of the fine black sand strip as shown in Figure 2.16 and Figure 2.17. Internal and external surcharge of 2 kPa were added. Bevameter testing was conducted following the procedure described previously, except rotation was stopped at 60 degrees to capture the soil conditions present at the identified failure condition. Data recording was then terminated, and the shear annulus and surcharge were removed. After shearing, the soil under the shear annulus was a mix of the SM and the fine black sand (Figure 2.18). To determine the depth of the shear zone, the soil was carefully removed using a trowel until the uniform black sand was revealed. The depth of the uniform black sand was measured against the height of the original soil surface. Sinkage was recorded during the test and the shear zone was calculated using Equation 2.

$$D_{sz} = D_{bs} - D_s \tag{2}$$

where D_{sz} is the depth of the shear zone, D_{bs} is the depth of the fine black sand, and D_s is the sinkage depth of the shear annulus at failure.

Shear zone testing was also conducted on CH at optimum water content and 85% of maximum standard proctor dry density. Under these conditions, the soil had sufficient strength to allow removal of a section of soil equal to that of the mold (described earlier in this section) which was subsequently filled with fine black sand. The same testing procedure was used for the CH as described previously for the SM.

3.3.10 Shear Strength Parameter Comparison

Additional geotechnical soil strength testing was conducted to measure strength parameters to compare to those measured by the bevameter. Six consolidated undrained triaxial tests (ASTM

D4767-11) and twelve direct shear tests (ASTM D 3080/D 3080M-11) were performed. Triaxial tests were conducted under effective confining stresses of 19.2 kPa, 38.6 kPa, and 58.7 kPa (same confining stresses as bevameter testing). Similar to bevameter tests, specimens were prepared at 85% of standard Proctor maximum dry density. Shearing was conducted at 1% strain/hour for 20 hours.

Three tests were conducted on identical samples at different effective stresses to obtain separate Mohr circles for manual fitting of a failure envelope to determine ϕ and *c*. Parameters were also generated using critical state soil analyses (Lambe and Whitman, 1969). Using least squares linear regression, stress paths were plotted in *p*-*q* space for data post-failure. Parameters *p* and *q* were calculated using the following equations:

$$p = \frac{\sigma_1 + \sigma_3}{2} \tag{3}$$

$$q = \frac{\sigma_1 - \sigma_3}{2} \tag{4}$$

where σ_1 is the major principal stress acting on the specimen and σ_3 is the minor principal stress. The line fit to *p*-*q* plots is referred to as the K_f-line. Parameters ϕ and *c* were calculated using the following equations:

$$\sin\phi = \tan\psi \tag{5}$$

$$c = \frac{b}{\cos\phi} \tag{6}$$

where ψ is the angle the K_f-line makes with the horizontal plane and *b* is the *q*-intercept of the K_f-line. A third method only applicable to cohesionless soils, known as the secant method, was also used. A single Mohr circle was plotted and a tangent line was fit to the circle through the origin to calculate ϕ.

Direct shear testing was conducted on the SM under similar stresses as the bevameter tests (normal stresses of 17.5 kPa, 38.6 kPa, and 58.7 kPa). Specimens were prepared at 85% standard

Proctor maximum dry density and sheared at a rate of 2 mm/minute until an axial strain of 20% was achieved.

Strength testing on a SP was conducted using direct shear and the bevameter. For direct shear testing, both soils (SM and SP) were prepared by pluviating soil into the shear box. The soils were air-dried and were not compacted. The SP was tested under the same normal stress as the SM direct shear tests. However, the SP was also tested under a fourth normal stress of 65.0 kPa to observe the shape of the failure envelope. SP specimens were sheared at the same rate and to the same strains as the previously described SM direct shear tests.

The SP was prepared for bevameter testing by pluviating the sand into a rectangular plastic container of dimensions 51 cm by 38 cm by 13 cm. A smaller container was used to reduce the volume of soil required for testing based on the results from shear plane testing (described subsequently). The shear annulus with sandpaper was paced in the center of the bin with an internal and external surcharge of 2 kPa (Figure 2.16).

4. Results and Discussion

3.4.1 Shear Interface and Surcharge Location Testing

Sinkage testing results for tests conducted on the SM are summarized in Figure 2.21 for varying shear interfaces (grousers, epoxied angular sand, and sandpaper) under different surcharge condition (no surcharge, external surcharge, and internal and external surcharge). Each of the curves in Figure 2.21 represents one of the three shear interfaces tested for a specific surcharge condition. Grousers consistently produced the greatest sinkage, with a sinkage of 47 mm for the no surcharge condition and 41 mm under external surcharge for a normal stress of 58.7 kPa. Sandpaper produced the least sinkage followed by the angular sand epoxied to the shear annulus.

Epoxied angular sand yielded 9 mm of sinkage with an internal and external surcharge, 18 mm of sinkage with an external only surcharge, and 26 mm of sinkage with no surcharge under a normal stress of 58.7 kPa. When sandpaper was used as the shear interface, sinkage of 18 mm, 13 mm, and 6 mm were observed for no surcharge, external only surcharge, and internal and external surcharge respectively under a normal stress of 58.7 kPa. An internal and external surcharge reduced sinkage most of the surcharge conditions tested.

With internal and external surcharge, ϕ varied with the shear surface tested. As shown in Table 2.3, the ϕ measured with sandpaper increased by 10 degrees with the introduction of an internal and external surcharge relative to the no surcharge condition. For epoxied sand, ϕ increased 8 degrees with the introduction of internal and external surcharge relative to the no surcharge condition. Grousers with an internal and external surcharge are not shown in Figure 2.21 because the sinkage of the shear annulus exceeded the free space between the internal surcharge and shear annulus. As displayed in Table 2.2, sandpaper under a 58.7 kPa normal stress with no surcharge experienced 29 mm less sinkage than grousers under the same conditions and 8 mm less sinkage than the angular sand under the same conditions. The sandpaper also exhibited much less sinkage than the other shear interfaces for 38.6 kPa and 19.3 kPa normal stress. Due to the reduced magnitude of slip sinkage, sandpaper was chosen as the preferred shear interface.

3.4.2 Surcharge Magnitude Testing

Figure 2.22 shows how sinkage varied with surcharge magnitude for sandpaper with an internal and external surcharge. Sinkage tests were conducted on the SM. With placement of a 2 kPa internal and external surcharge, sinkage was reduced by 18 mm compared to the no surcharge condition. However, with increasing surcharge, the additional reduction in sinkage observed was

minimal. Sinkage was only reduced by an additional 2 mm with the introduction of up to 6 kPa surcharge. Given the minimal effect of increased surcharge, a 2 kPa surcharge was selected for use in the field to reduce the required surcharge dead weight from 42 kg to 7 kg.

3.4.3 Sinkage-Measurement Reproducibility Testing

To better understand test reproducibility, eleven replicate tests were conducted with an internal surcharge of 2 kPa and an external surcharge of 2.6 kPa. These tests produced sinkage ranging from 0.3 mm to 3.8 mm with an average of 1.7 mm of sinkage and a standard error of 0.3 mm. The eight tests conducted on an internal and external surcharge of 2 kPa produced sinkage values ranging from 0.6 mm to 4.3 mm with an average of 2.6 mm of sinkage and a standard error of 0.4 mm. A histogram of the sinkage measured from these tests can be found in Figure 2.23. All other tests were replicated 4 times and average sinkage values along with standard error for each test are reported in Table 2.5. Sinkage reproducibility testing demonstrated general agreement between sinkage values, indicating reliability of sinkage results used for shear interface and surcharge location method determinations.

3.4.4 Shear Zone Testing

The depth of the shear zone is important for understanding the location of the measured shear strength in bevameter field testing and the minimum sample size required for laboratory testing. If the location of the induced failure plane is known, bevameter field tests can target the layer of interest. Figure 2.24 presents the results of sinkage and shearing depth for three tests conducted under different normal stresses on air-dried SM. Thickness of the shear zone in SM under a normal stress of 58.7 kPa and an internal and external surcharge of 2 kPa ranged from 6 mm to 10 mm with an average shear zone thickness of 8.5 mm.

Shear zone testing was conducted on a CH to better understand the depth of the shear zone in a clay. For the CH, the failure plane developed at the surface of the shear annulus under a normal stress of 58.7 kPa and an internal and external surcharge of 2 kPa.

As a result of shear zone testing, a reduced sample size for laboratory testing was adopted and a preliminary understanding of the approximate depth of shear strength measurement for two soils was gained. Reducing the bevameter sample size lessens the volume of soil required for testing, making bevameter laboratory testing less time consuming and more practical for collection of laboratory prepared soils.

3.4.5 Shear Strength Parameter Comparison

A comparison of shear stress at failure for SM by bevameter tests, consolidated undrained triaxial tests, and direct shear tests, is provided in Figure 2.26 Bevameter testing yielded consistently lower ϕ and similar c when compared to triaxial and direct shear tests conducted on SM. The variability in parameters generated by triaxial testing on SM is shown in Table 2.6. Triaxial data is known to produce varying results depending, in part, on the data analysis technique used (Bowles, 1992). Each set of triaxial data was analyzed using three different methods: Lambe's K_f-method, best fits to Mohr circles, and secant analysis (assuming $c = 0$). Friction angle for the SM varied from 27 degrees to 46 degrees for the different data analysis techniques used. The Mohr circle analysis involves judgment that can result in a large error (Oravec, 2009) with friction angle ranging from 30 to 38 degrees for the SM. The secant method also yielded inconsistent results (due to a lack of averaging method for varying normal stresses), with ϕ ranging from 33 degrees to 46 degrees. Therefore, parameters generated using the K_f-method were used for comparison in this study. The K_f-method was selected to eliminate user judgment in determination of the failure

envelope. Using Lambe's K_f method, an average ϕ of 39 degrees for triaxial results on SM was used for comparison to ϕ measured using the bevameter.

Direct shear tests on SM at varying moisture contents (S = 0% to S = 100%) are shown in Table 2.7. Direct shear analysis on SM yielded an average ϕ of 40 degrees. This finding is consistent for the data collected from direct shear and triaxial tests on SM. As noted by Bowles (1992), sands with ϕ less than 35 degrees have been observed to have negligible differences between direct shear and triaxial data. However, for sand with ϕ greater than 35 degrees, direct shear tends to have a ϕ 1 to 4 degrees greater than the ϕ measured by triaxial tests (Bowles, 1992).

Bevameter testing on the SM generated an average ϕ of 34 degrees, approximately 5 degrees less than triaxial tests and 6 degrees less than direct shear tests. This phenomenon has been observed by others and some have argued the triaxial and direct shear test do not produce stress and failure conditions that are representative of bevameter test conditions or vehicle thrust (Bekker, 1969; Edwards et al., 2017). In 1991, a review of methods used to measure soil strength for vehicles concluded that the bevameter was the method that most closely simulates vehicle motion (Okello, 1991). The review discussed non-representative soil structure and failure planes in laboratory tests and noted the most representative methods were those that could be conducted in-situ to minimize soil disturbance (Okello, 1991). Bevameter testing also allows failure along the weakest plane, while direct shear and triaxial testing control or have stress-preferred failure planes, respectively, based on the test setup.

Senatore and Iagnemma (2011) discuss why shearing devices which produce small displacements may not be appropriate for vehicles. The study noted a 5 m long tank track slipping at 10 percent generates a displacement of 500 mm, which is far beyond the displacement generated by a direct shear or triaxial test (Senatore and Iagnemma, 2011). The bevameter shear test is

conducted up to 400 mm radial displacement as compared to approximately 13 mm and 15 mm of ultimate axial displacement for direct shear and triaxial tests, respectively. Failure in bevameter tests conducted on SM in this study was defined at 66.7 mm average annular displacement (60 degree angular displacement) compared to triaxial tests conducted on SM which suggested failure occurred between 0.8 mm and 1.6 mm axial displacement (1.5% to 3% axial strain) and about 1.6 mm for direct shear (2.5% strain). While the displacements that peak shear stress occurs beneath a wheel or track has not been studied in detail, the difference between displacements at peak shear stress in bevameter tests, and triaxial and direct shear tests is substantial. As discussed in the Background section of this chapter, the failure mechanisms of triaxial and direct shear are much different than that of the bevameter. For these reasons, the bevameter is generally recommended as the preferred method for the measurement of terramechanics relevant surficial soil strength (Bekker, 1969; Okello, 1991; Edwards et al., 2017).

As shown in Figure 2.25, the direct shear tests conducted on SP demonstrated near-linear behavior and bevameter tests conducted demonstrated non-linearity of the failure envelope. Similarly, Figure 2.26 displays the shear stress at failure for direct shear, triaxial, and bevameter tests under varying normal stresses on an SM. The data illustrates agreement between all three tests at shear stresses near 20 kPa. However, as shear stress increases bevameter data deviates from the linear behavior of the triaxial and direct shear tests. Bailey and Webber (1964) compared parameters generated from triaxial and bevameter testing on a sandy and clayey soil and concluded the failure envelope produced from triaxial testing exhibited linear behavior over the stress range while rotational shear testing yielded non-linearity of the failure envelope. Non-linearity is believed to be more representative of vehicle soil interaction (Bekker, 1969). However, further

testing is required to compare these results to the failure envelope produced by vehicles on this soil.

5. Summary and Conclusion

Bevameter testing was conducted to evaluate the effect shear interface (grousers, epoxied angular sand, and sandpaper) had on sinkage and shear strength parameters when tested on a SM. A LVDT was added to a human-powered bevameter to measure sinkage. Internal and external surcharge locations were tested to observe the impact no surcharge, external only surcharge, and internal and external surcharge had on shear annulus sinkage in a SM. Shear zone testing was conducted to observe the depth the shear zone extends into a SM and CH. Sinkage reproducibility tests were conducted in a SM to analyze the consistency of bevameter sinkage values for verification of sinkage values produced in shear interface, surcharge location, and surcharge magnitude testing. Parameters generated by the bevameter on a SM and a SP were compared against triaxial tests and direct shear tests. From these studies, the following conclusions can be made:

1. Sandpaper is recommended as a shear interface compared to coarse angular sand epoxied to the annular plate and metal grousers. Sandpaper exhibited the least sinkage during shear testing. By reducing the effects of slip-sinkage, the failure plane is returned to a location sufficiently close to the shear annulus for determination of shear strength parameters. This allows the tester to know the shear stress on the failure plan to generate accurate strength parameters from test data.
2. Use of a 2 kPa surcharge internal and external to the shear annulus with sandpaper as the shear interface reduces sinkage from 18 mm to 6 mm in a SM under a normal load of 58.7 kPa. Lower sinkage occurs for tests conducted at lower normal stresses under the conditions tested.

An efficient internal and external surcharge of 2 kPa can be used to reduce sinkage of the shear annulus while minimizing the amount of reactive force (dead weight) required for surcharge in bevameter field testing for similar soils.

3. Repeated tests to measure sinkage of the bevameter shear annulus during shear testing with sandpaper show general agreement, with a standard error of 0.4 mm for testing conducted on a SM with internal and external surcharge of 2 kPa under a normal stress of 58.7 kPa. The low error produced by sinkage reproducibility tests verify the shear interface, surcharge location, and surcharge magnitude sinkage results used for the development of the revised bevameter procedure.
4. Lower ϕ and similar c were observed for shear strength parameters measured for a SM by the bevameter compared to those measured by triaxial and direct shear tests. Repeated tests on a SP show non-linearity of the failure envelope for bevameter tests and near-liner behavior for direct shear failure envelopes.
5. Because the field-focus bevameter is human powered, consistent shear rates can be difficult to accurately replicate, introducing uncertainty to shear rate studies. A fully automated bevameter should be used to study the affect shear rate has on the measurement of surficial shear strength parameters. Additionally, the nonlinearity of the bevameter failure envelope should be further studied to determine the optimum testing normal stress range for measurement of vehicle-representative soil strength.

6. Tables and Figures

Table 2.1. Soil properties for Filter Sand, ERC Clay and Silica Sand.

Soil Property	ASTM Method	Filter Sand	ERC Clay	Silica Sand
USCS Classification	D 2487 - 17	SM	CH	SP
USDA Classification	N/A	Sand	Clay	Sand
Liquid Limit	D 4318 -17el	N/A	50.4	N/A
Plastic Limit	D 4318 -17el	N/A	19.0	N/A
Specific Gravity	D 854 - 14	2.7	2.67	-
Max. Dry Unit Weight (kN/m^3)	D 689 - 12e2	16.3	15.4	-
Target Dry Unit Weight (kN/m^3)	N/A	13.8	13.3	-
Optimum Water Content (%)	D 689 - 12e2	12.7	21.4	-

N/A = Test not required for classification; - = testing not preformed

Table 2.2. Sinkage of the shear annulus at 60 degree rotation in a SM for sandpaper, angular sand, and grousers, under no surcharge, external surcharge, and internal and external surcharge conditions.

Material	Normal Load (kPa)	No Surcharge Sinkage (mm)	External Surcharge Sinkage (mm)	Internal and External Surcharge (mm)
Sandpaper	19.3	10.9	6.6	2.5
	38.6	14.5	10.9	4.3
	58.7	17.8	12.7	6.1
Angular Sand	19.3	15.2	10.9	5.1
	38.6	20.1	13.5	8.1
	58.7	25.9	18.3	8.6
Grousers	19.3	30.7	11.6	-
	38.6	35.0	27.5	-
	58.7	46.9	41.0	-

Table 2.3. Shear strength parameters for a SM under varying surcharge conditions and shear surfaces.

Material	Surcharge Condition	Friction Angle, ϕ (degrees)	Cohesion, c (kPa)
Grousers	No Surcharge	24	0
	External Surcharge	31	7.5
	Internal and External Surcharge	-	-
Angular Sand	No Surcharge	24	1.8
	External Surcharge	32	0
	Internal and External Surcharge	32	0
Sandpaper	No Surcharge	24	0
	External Surcharge	34	0
	Internal and External Surcharge	34	2.5

Table 2.4. Shear zone thickness for tests at varying normal stresses conducted on a SM.

Normal Stress (kPa)	Shearing Depth (mm)	Sinkage Depth (mm)	Shear Zone (mm)
19.3	8.9	6.9	2.0
38.6	7.6	5.1	2.5
58.7	17.8	11.4	6.4
58.7	11.4	3.3	8.1
58.7	17.5	7.7	9.8
58.7	18.3	8.6	9.7

Table 2.5. Average sinkage values and standard error for sinkage reproducibility testing conducted on an SM under a normal stress of 58.7 kPa.

Internal Surcharge (kPa)	External Surcharge (kPa)	Average Sinkage (mm)	Error (mm)
0	0	20.4	3.7
2	2.6	1.7	0.3
4	5.6	1.4	0.9
6	8.7	1.3	0.4
2	2	2.6	0.4
4	4	1.1	0.5
6	6	0.4	0.1

Table 2.6. Consolidated undrained triaxial results for SM specimens analyzed using different methods.

Test	Failure Criterion	Friction Angle, ϕ (degrees)	Cohesion, c (kPa)
FS_E1	K_f Line	37	9.5
FS_E1	Mohr-Coulomb	30	8.6
FS_E1	Secant	37, 39, 39	0
FS_E2	K_f Line	40	0
FS_E2	Mohr-Coulomb	38	2
FS_E2	Secant	46, 41, 33	0
Pauly (2019)	Secant	27	0

Table 2.7. Direct shear results for SM conducted under various water content conditions.

Test	Saturation, S (%)	Friction Angle, ϕ (degrees)	Cohesion, c (kPa)
DS_E13	0	42	0
DS_E8	0	43	0.7
DS_E12	0	43	0
DS_E10	0	44	0
DS_E11	0	44	0
DS_E9	0	45	0
DS_E3	20	30	8.1
DS_E1	22	31	7.0
DS_E2	25	34	6.0
DS_E6	100	38	0.3
DS_E4	100	36	3.4
DS_E5	100	35	1.8

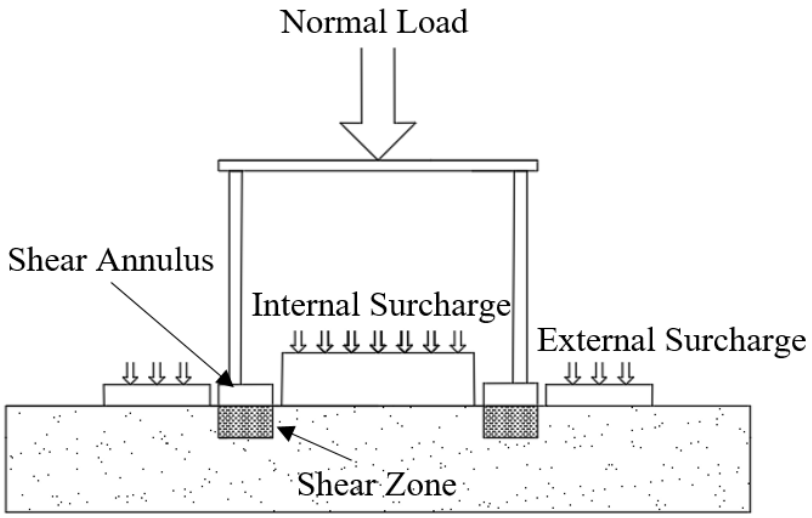

Figure 2.1. Cross section of shear annulus showing shear zone underneath the shear annulus in bevameter testing.

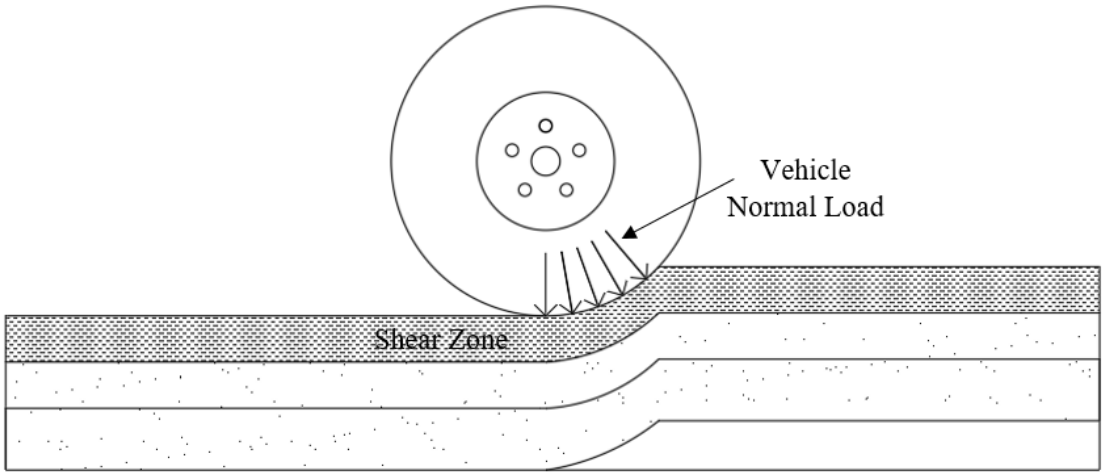

Figure 2.2. Cross section of the shear zone underneath a wheeled vehicle.

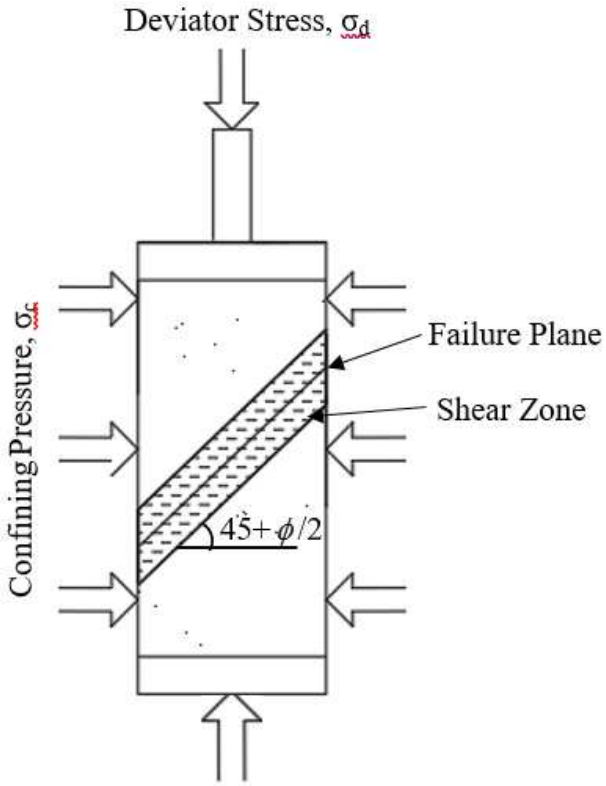

Figure 2.3.Triaxial specimen with failure plane at an angle of $45+\frac{\phi}{2}$ to the horizontal plane.

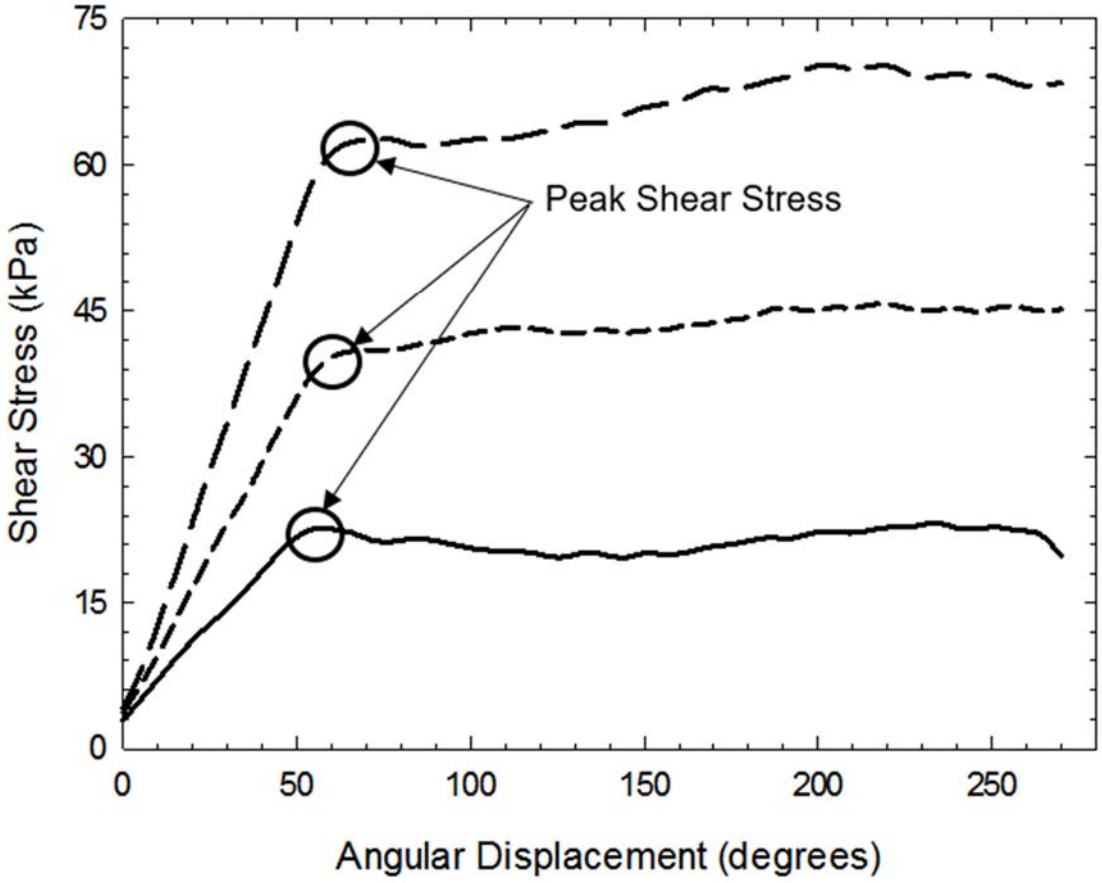

Figure 2.4. Example bevameter shear data for shear stress versus angular displacement (Pauly, 2019).

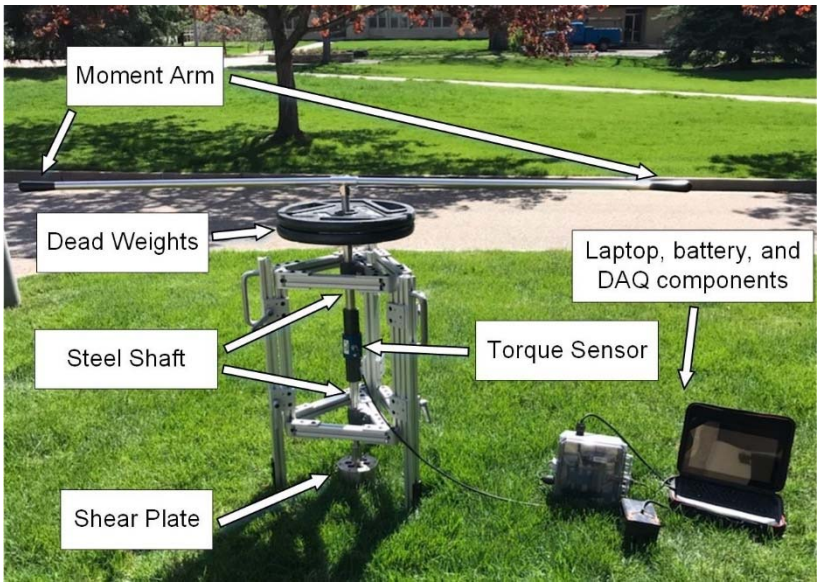

Figure 2.5. Field-focused bevameter setup (Pauly, 2019).

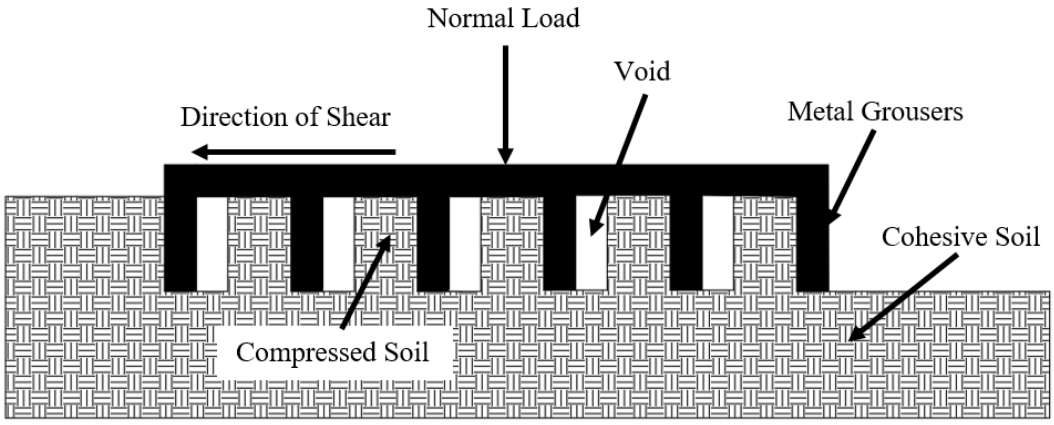

Figure 2.6. Soil flow caused by grouser shearing in a cohesive soil.

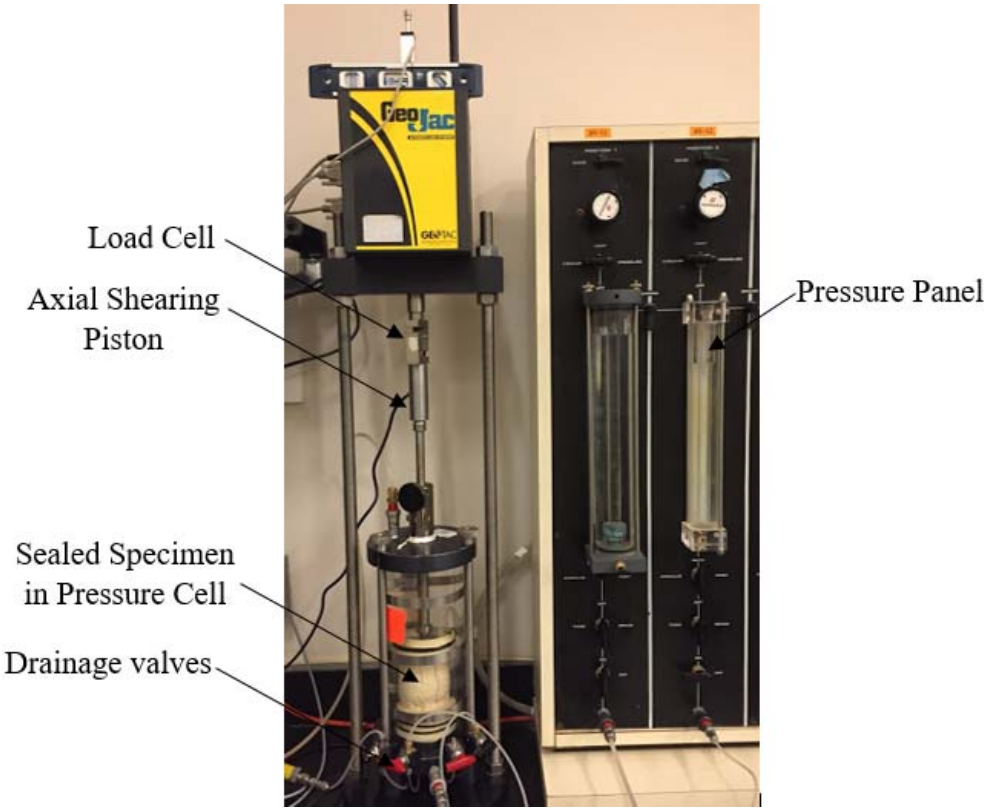

Figure 2.7. Triaxial specimen placed in shearing apparatus.

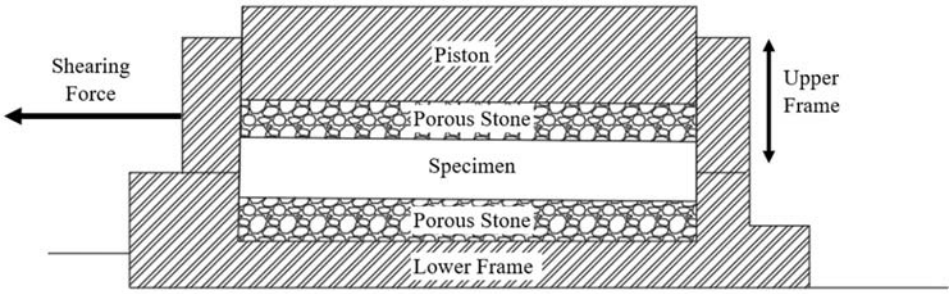

Figure 2.8. Direct shear box (ASTM D 3080/D 3080M-11, 2011).

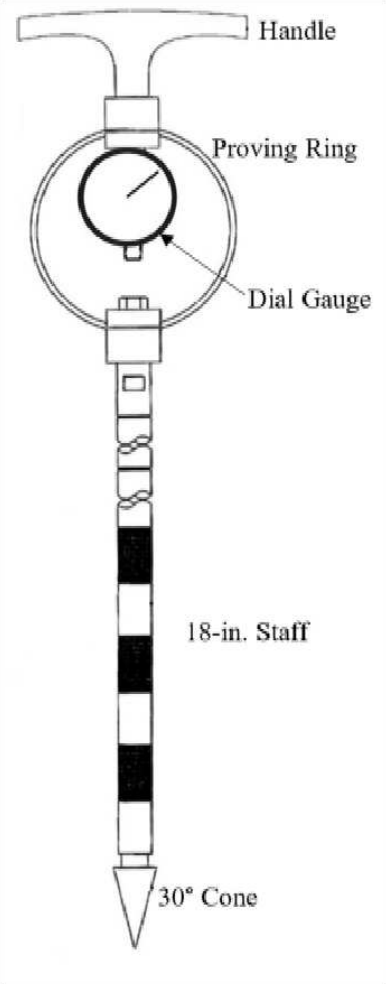

Figure 2.9. Humboldt Manufacturing Co. Corps of Engineers Cone Penetrometer (Humboldt, 2011).

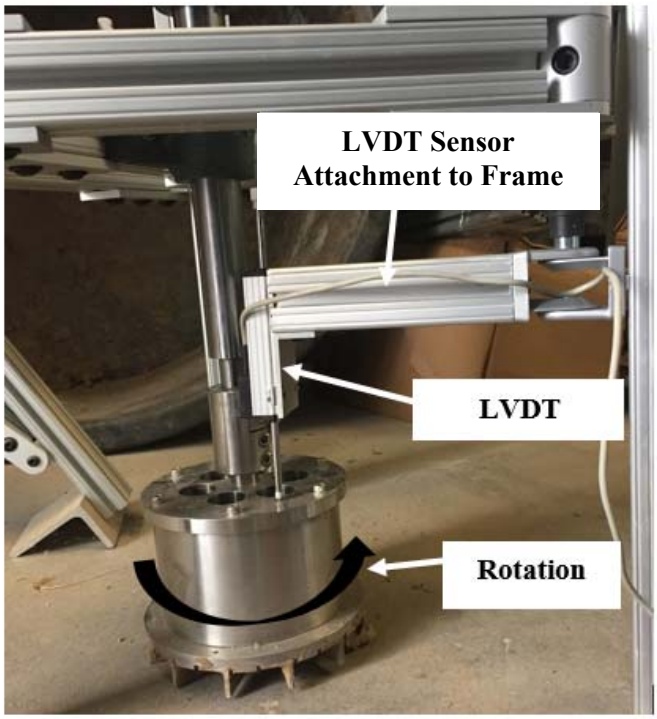

Figure 2.10. LVDT sensor attached to bevameter frame.

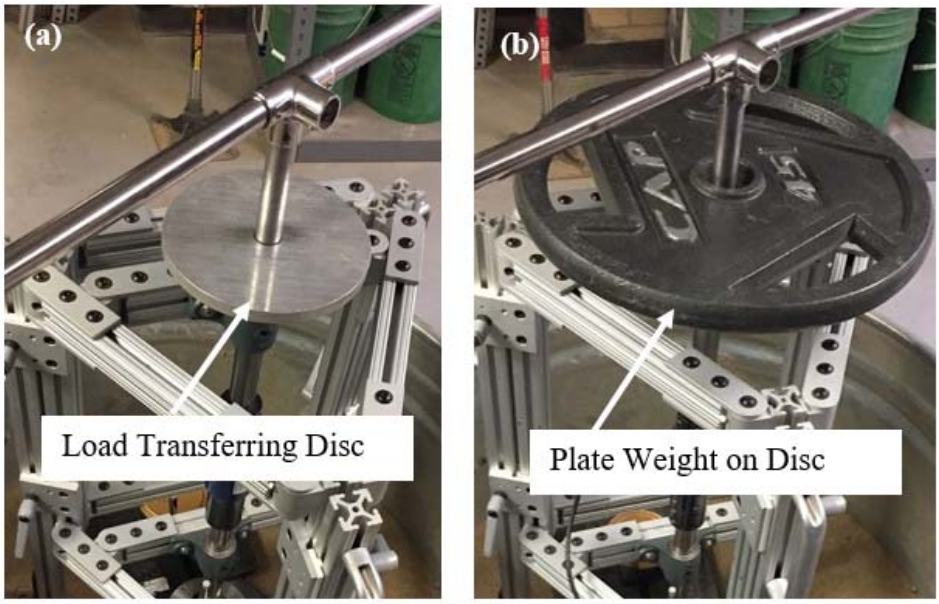

Figure 2.11. (a) Disc designed to transfer loading to shaft, and (b) weight plate placed on disc.

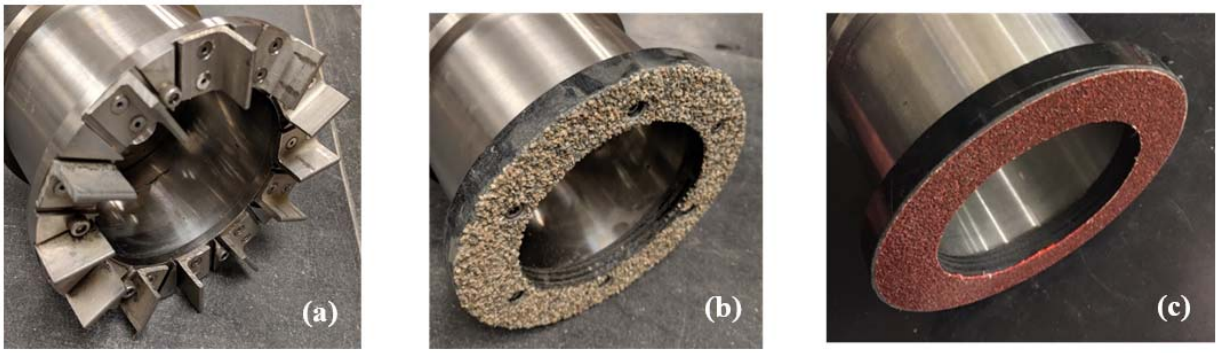

Figure 2.12. (a) Grousers, (b) epoxied angular sand, (c) adhesive sandpaper.

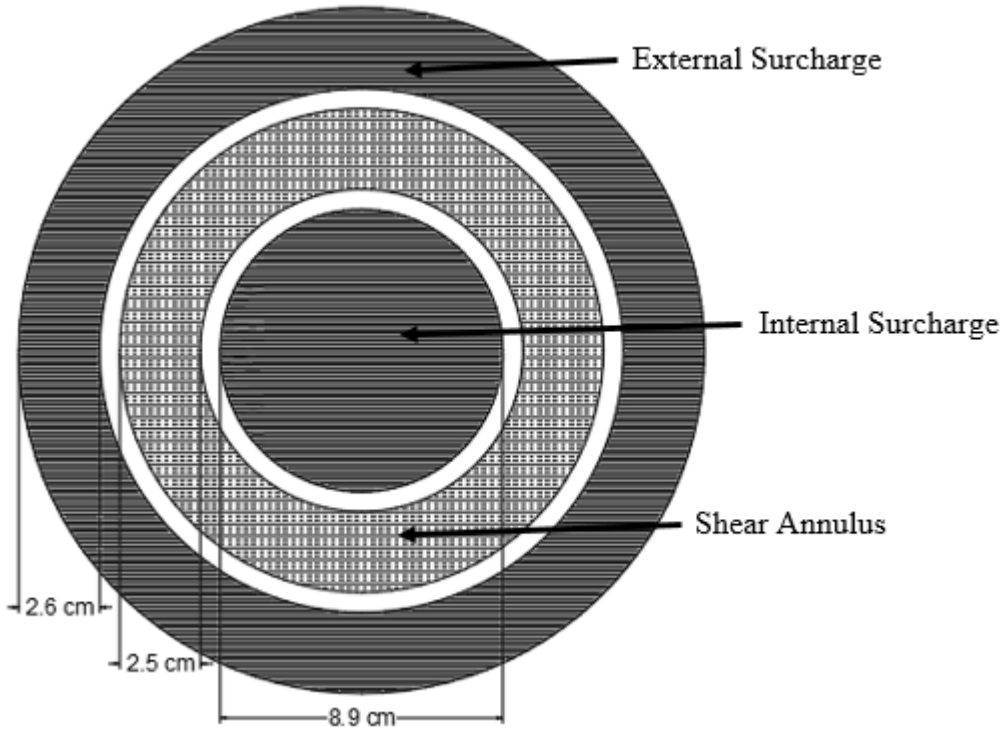

Figure 2.13. Positions of internal and external surcharge with reference to the shear annulus.

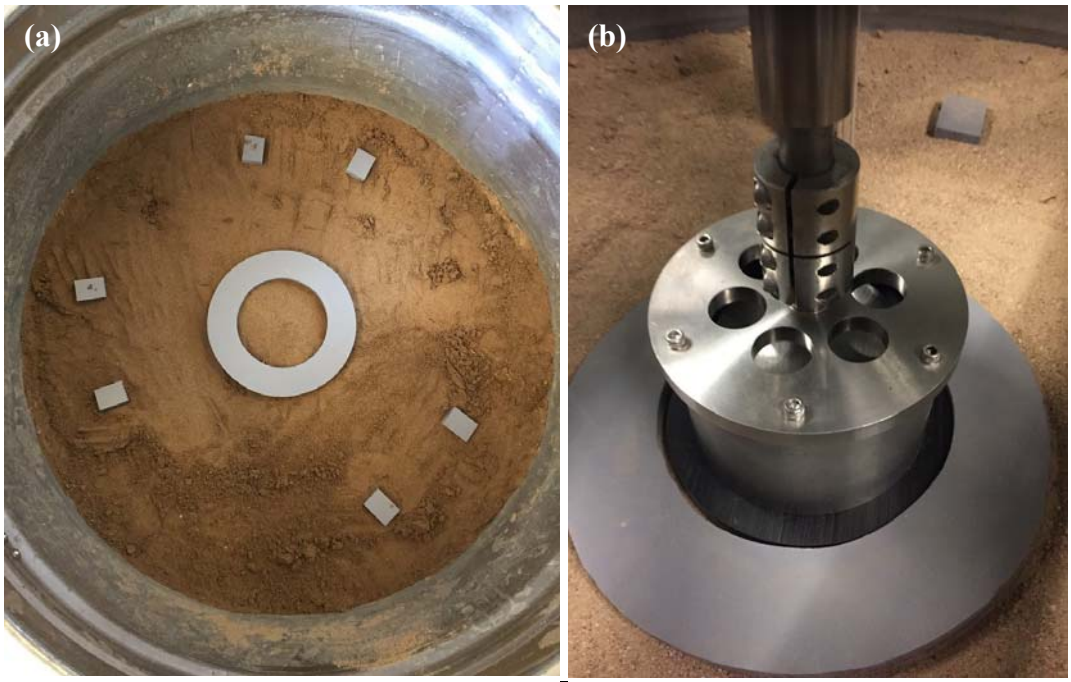

Figure 2.14. (a) Plastic surcharge ring and supporting blocks (b) surcharge ring with shear annulus placed in the center.


Figure 2.15. SM (left) and fine black sand (right).

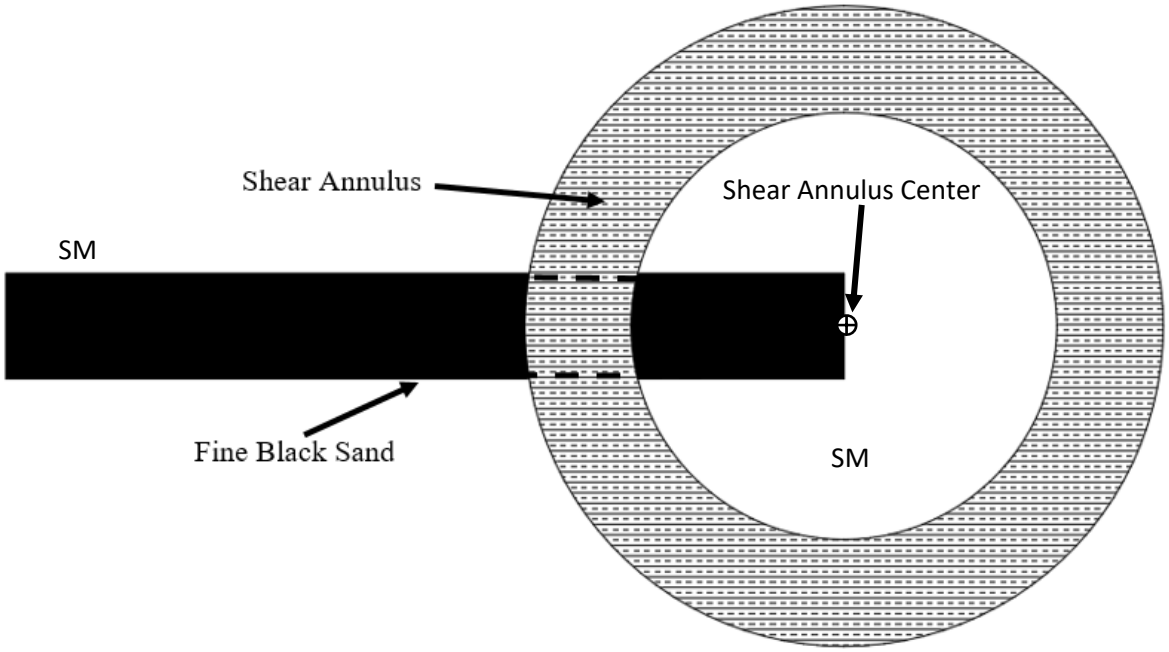

Figure 2.16. Shear annulus placement with respect to fine black sand.

Figure 2.17. Placement of shear annulus and external surcharge ring on SM for shear zone testing.

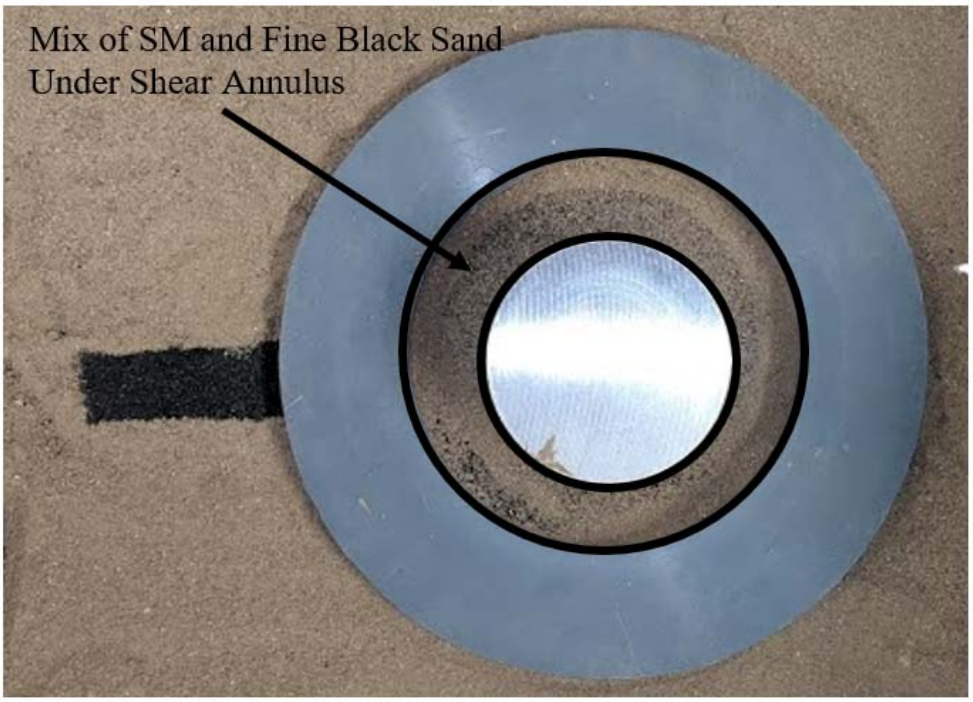

Figure 2.18. Mixture of SM and fine black sand under shear annulus after shearing.

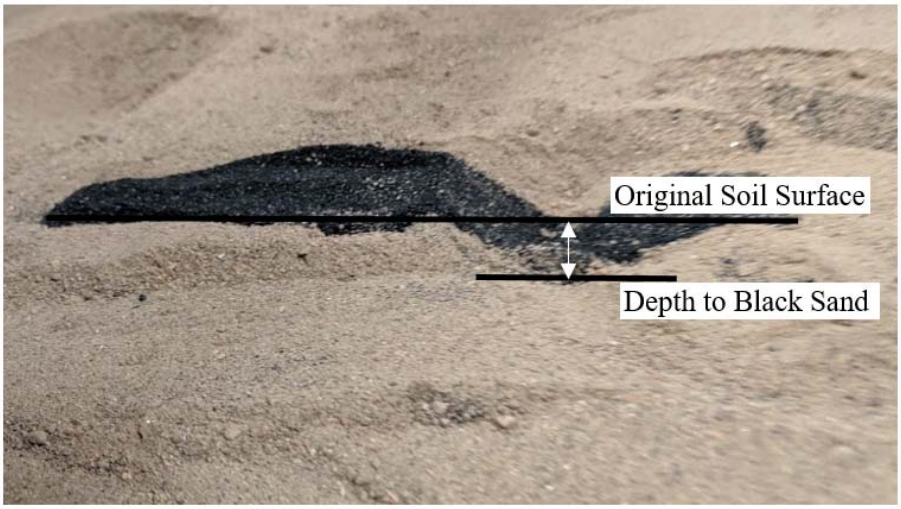

Figure 2.19. Measurement of shear zone for SM under a normal stress of 58.7 kPa.

Figure 2.20. Shear annulus placed on a CH in plastic bin with an internal and external surcharge of 2 kPa.

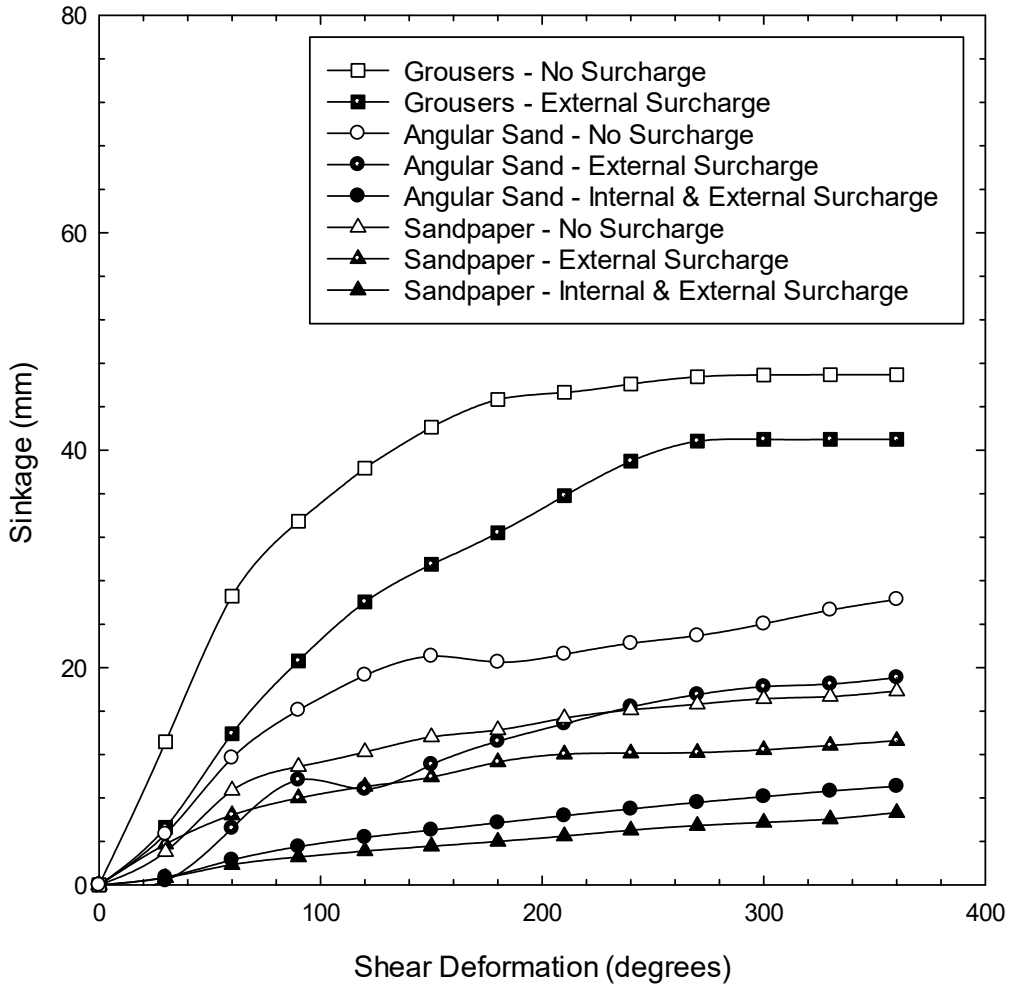

Figure 2.21. Sinkage versus shear deformation for grousers, epoxied angular sand, and sandpaper under no surcharge, external surcharge, and internal and external surcharge tested under a normal stress of 58.7 kPa in a SM.

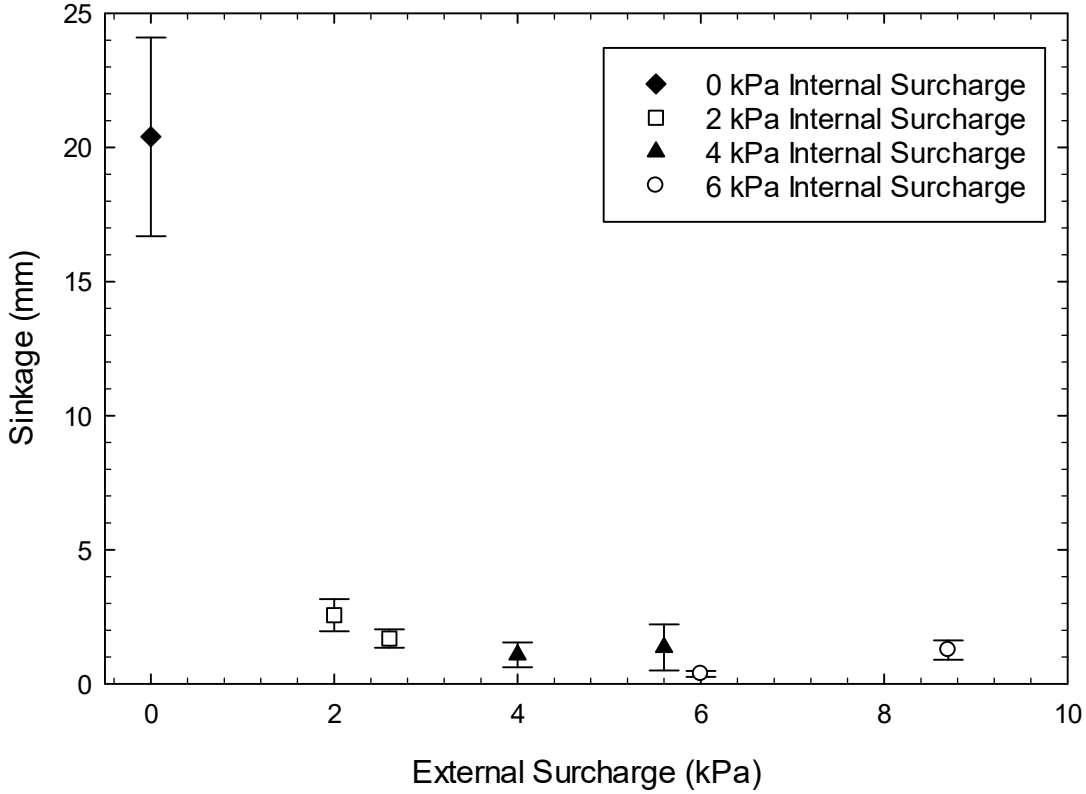

Figure 2.22. Sinkage versus external surcharge for internal surcharges of 0, 2, 4, and 6 kPa tested under a shear annulus normal stress of 58.7 kPa in a SM.

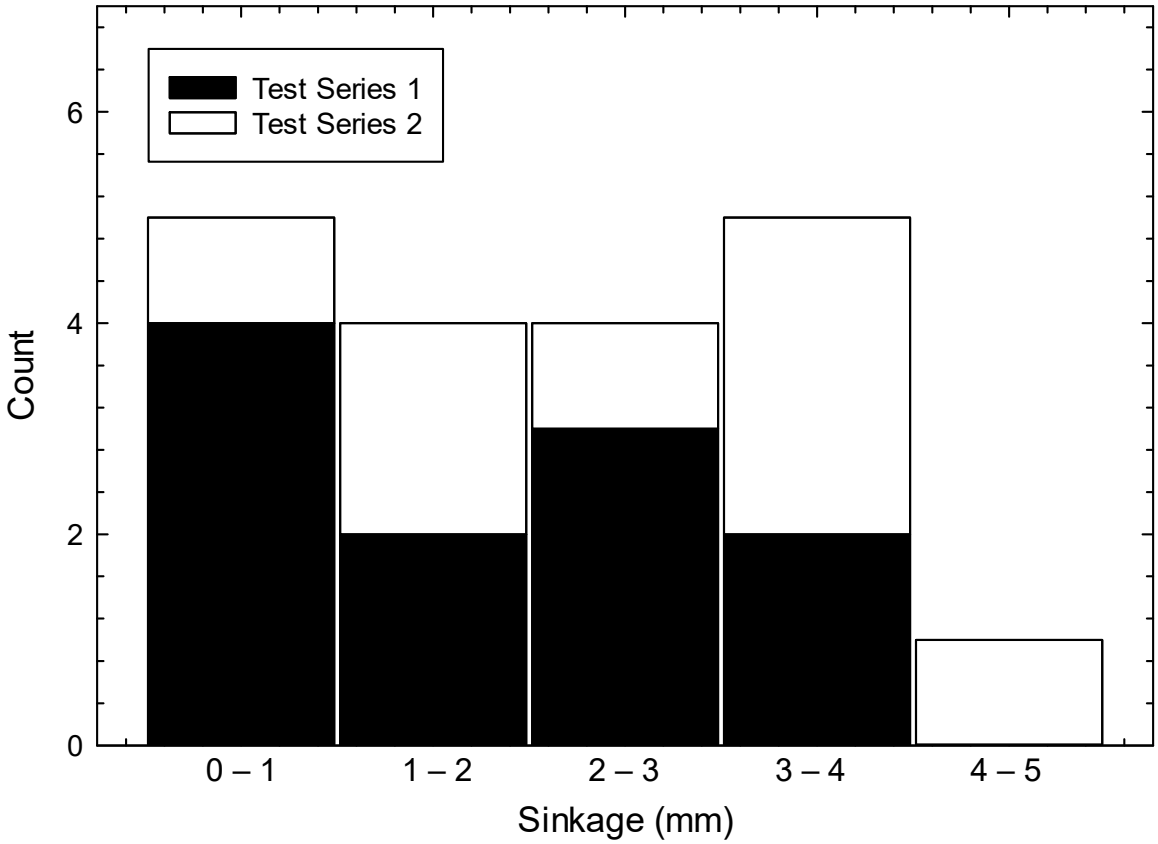

Figure 2.23. Histogram for sinkage repeatability study conducted on a SM using sandpaper under a normal stress of 58.7 kPa for two testing series; Series 1 was conducted with an internal surcharge of 2 kPa and an external surcharge of 2.6 kPa and Series 2 was conducted with an internal and external surcharge of 2 kPa.

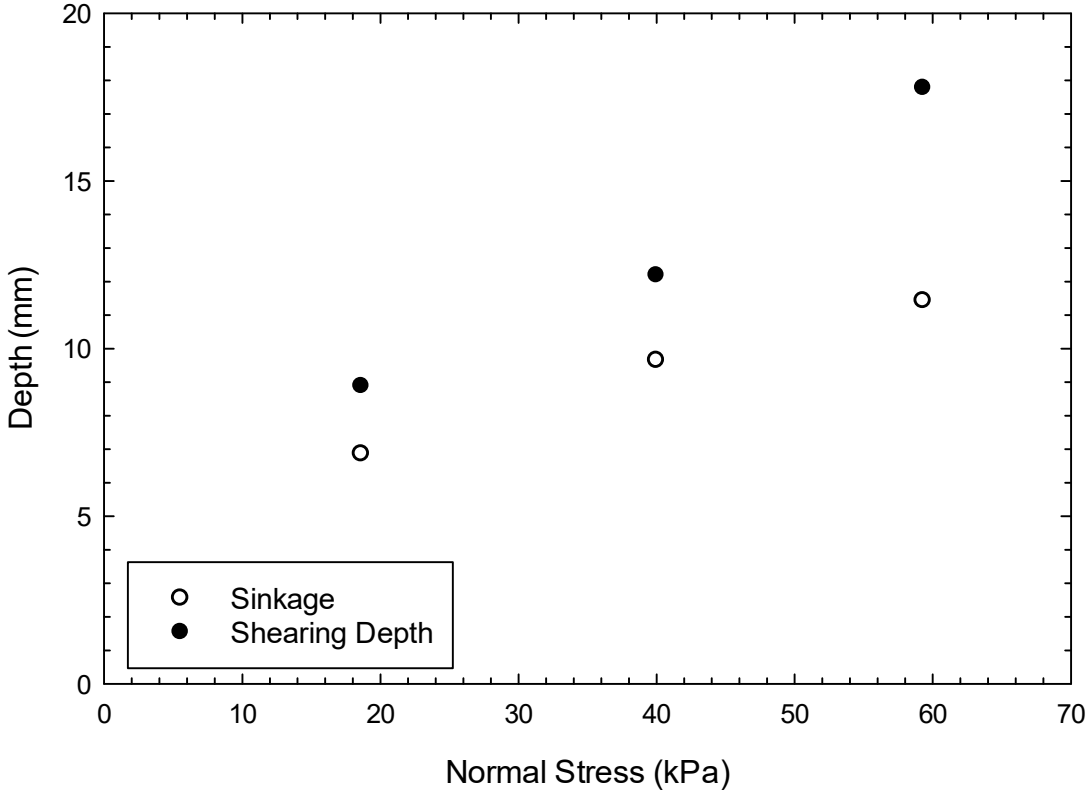

Figure 2.24. Sinkage depth and shear zone depth versus normal stress for air-dried SM.

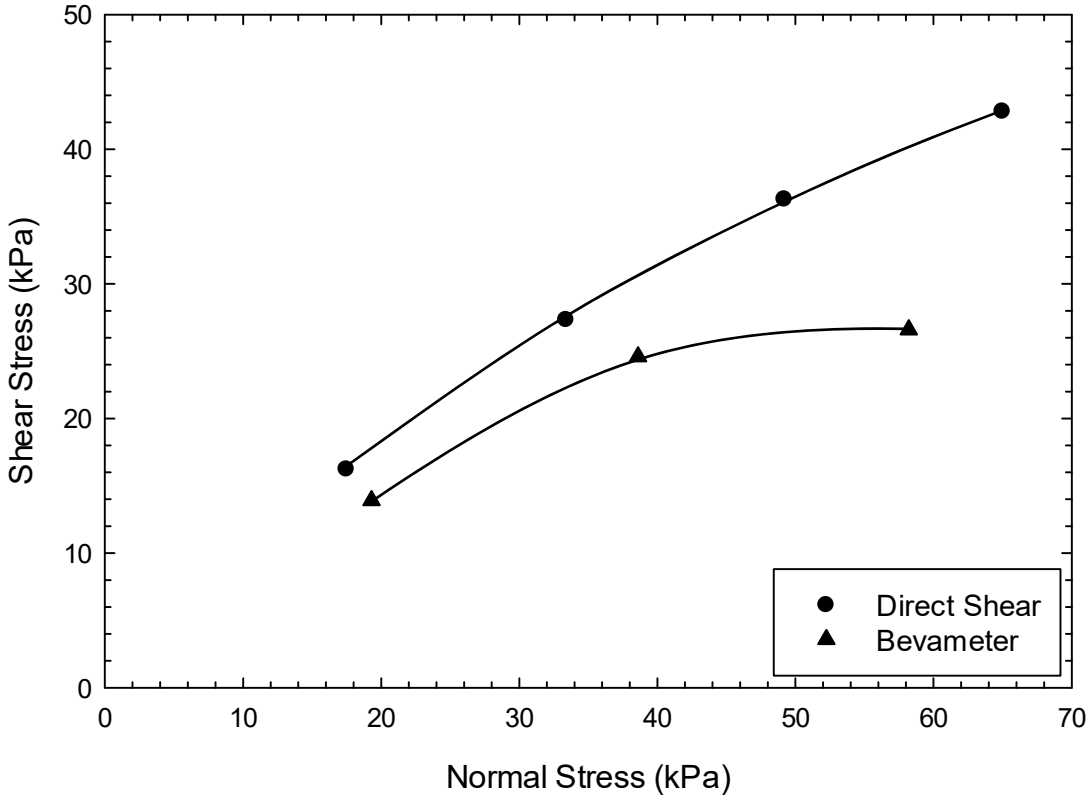

Figure 2.25. Shear stress versus normal stress for a SP tested by the bevameter and direct shear apparatus.

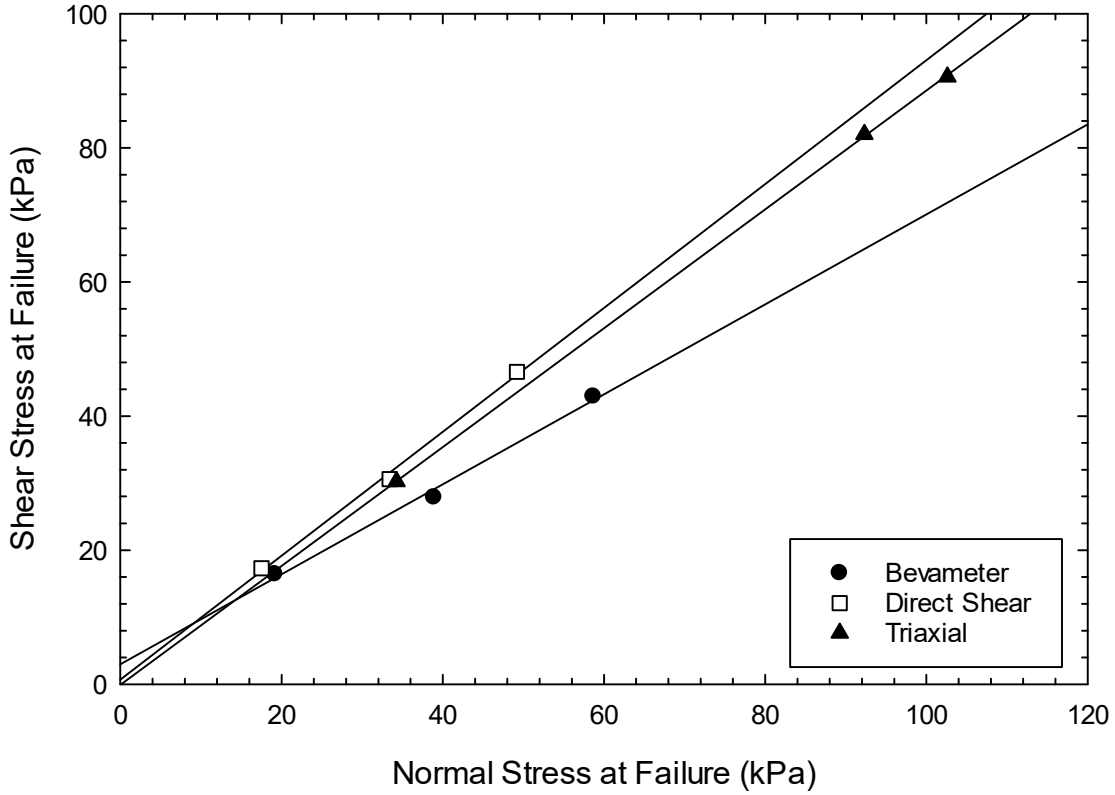

Figure 2.26. Shear stress versus normal stress at failure for direct shear, bevameter, and triaxial testing on SM with failure envelopes found using method of least squares linear regression.

3. STRESS MODEL EVALUATION

1. Introduction

Understanding the properties that contribute to soil strength is critical for predicting vehicle mobility across terrain. Terramechanics models rely on soil strength for accurate prediction of speed made good and go/no-go vehicle routing maps. In state-of-practice terramechanics models, a simple metric (such as the RCI-VCI comparison) is used to empirically predict vehicle mobility. These empirical relationships have numerous limitations, and in many cases, show poor correlation to variables related to vehicle performance (Williams et al., 2017). The Bekker method provides a more comprehensive description of soil behavior, and parameters measured using a bevameter can be used for input into physics-based soil strength models (viz complex terramehanics models; Choi et al., 2019). However, physically based soil strength models have only begun to receive more attention in recent years (Bradbury et al., 2016). As discussed in Chapter 2, the bevameter is the preferred method for measuring in-situ surficial soil strength. However, for most applications, extensive testing using the bevameter may not be feasible or may be too dangerous for military operations. For these reasons, the prediction of surficial soil strength parameters using data from remote sensing is necessary to modernize spatial predictions of soil strength parameters.

Pauly (2019) describes the development of the Strength of Surface Soils (STRESS) model, which predicts surficial soil strength using fine scale soil moisture and soil texture data. As shown in Figure 3.1, the STRESS model calculates soil strength properties as a function of soil texture from remote sensing data and soil moisture from the Equilibrium Moisture from Topography, Vegetation, and Soil (EMT+VS) model. The EMT+VS model conducts a water balance of the hydrologically active soil layer, considering infiltration, deep drainage, lateral flow, and

evapotranspiration. The STRESS model estimates effective ϕ and c_θ from soil texture and apparent c from a closed-form equation used to calculate suction stress (Lu et al., 2010). The outputs from the STRESS model are ϕ and c_θ. However, the model performance is believed to be hindered by a lack of near-surface soil strength pedotransfer functions (Pauly, 2019).

The objective of this study is to evaluate the performance of the STRESS model using a field-focused bevameter at a field site in northeastern Colorado. In-situ soil strength was measured at nine locations. Bevameter testing was completed at three normal stresses at each testing location using coarse sandpaper as the shearing interface with an internal and external surcharge of 2 kPa. Soil moisture was collected at 21 locations and used as input into the EMT+VS model to predict fine-resolution patterns of soil moisture. The STRESS model was run using interpolated soil textural data and downscaled soil moisture data from EMT+VS (data from McCutcheon, 2006; interpolation described in Pauly, 2019). The soil strength data recorded using the bevameter was evaluated to determine ϕ and c_θ at the nine testing locations. Parameters generated from bevameter data were compared to soil strength outputs from the STRESS model. The performance of the STRESS model is discussed.

2. Background

Existing U.S. Military and NATO models predict soil moisture and soil strength for estimation of vehicle performance across terrain in terms of RCI. However, RCI is useful for vehicle mobility predictions only when VCI is known. Many vehicles have not been studied for determination of VCI. As a result, the usefulness of soil strength parameters predicted based on remote sensing data is limited when using the empirically derived RCI framework. Additionally,

complex physics-based terrain computer simulations require physics-based soil strength information not provided by the RCI framework.

The STRESS model uses soil moisture and soil texture to estimate parameters which are equivalent to Bekker total stress strength parameters (Pauly, 2019). The STRESS model can use soil moisture inputs from the EMT+VS model or from measured soil moisture data, and fine resolution soil texture data from datasets such as SSURGO (Soil Survey Staff, 2018) or from local measured values of soil texture data (percentage sand and clay by mass). The STRESS model predicts soil strength parameters using Lu's method to calculate effective stress in unsaturated soils by estimation of suction stress (Lu et al., 2010). Lu's method employs van Genuchten's soil water retention parameters, which are estimated using empirical relationships based on soil texture (Schaap et al., 2001; van Genuchten, 1980). The STRESS model uses percentages of sand, silt, and clay from United States Department of Agriculture (USDA) classifications to crosswalk to USCS soil classifications (García-Gaines and Frankenstein, 2015). The model predicts effective stress strength parameters using the determined USCS class average values. The model calculates c_θ by adding apparent c from Lu's method to the estimated effective c from class average values. A full description of the STRESS model setup, calibration, and input parameters can be found in Pauly (2019).

Pauly (2019) evaluated the STRESS model and determined the model captures the approximate magnitude of Bekker strength parameters when compared to strength parameters measured using the bevameter. A three-day field-testing campaign revealed the bevameter did not capture the effects of suction stress and Pauly (2019) recommended adjusting the bevameter field methodology to capture true soil strength behavior to better tests the ability of the STRESS model to predict soil strength. Pauly (2019) also concluded the generality of the binned parameters used

for soil strength estimation limits the performance of the model. The performance of the model is expected to improve if binned parameters are replaced with pedotransfer functions that directly relate soil texture to effective shear strength parameters (Pauly, 2019). However, to develop such a database, a standardized testing procedure is needed (such was the motivation for the work described in Chapter 2).

Efforts have been made to compile existing soil strength data collected from a bevameter for improvement of soil strength models (Balling et al., 2019). However, many of these datasets are not consistent in strength measurement procedure and only test one or two soil textures. For these reasons, the development of a comprehensive database using the bevameter is recommended to improve the performance of the STRESS model.

3. Methods and Materials

3.3.1 Drake Farm Field Site

The Drake Farm field site has an area of 109 ha with an elevation ranging from 1559 m to 1588 m and is in Northeastern Colorado. The site has slopes ranging from 0% to over 13% (Figure 3.2) and was farmed in a wheat-fallow crop rotation for several decades before being transitioned to a Conservation Reserve Program (CRP) site in 2013. In 2013 and 2014 a native grass blend was planted. Figure 3.2 shows the former strip-cropping pattern which can still be observed in the vegetation. The near-surface site soils are aeolian silt and sands. However, the site has been extensively tilled, making the soil patterns unrepresentative of natural soil deposition. A detailed description of the site can be found in Green et al. (2009) and Green and Erskine (2011). Figure 3.3 shows 21 sampling locations which were selected for soil moisture measurement; nine of these locations were selected for soil strength sampling using the bevameter.

3.3.2 Soil Moisture Sampling

At each field-testing location, an average moisture over the top 50 mm of soil was measured using a POGO HydraProbe portable soil moisture measurement device (Stevens Water Monitoring Systems, Inc., Portland, OR, USA). An area approximately 50 mm in diameter was cleared on the soil surface at each soil moisture sampling location. Surface debris was removed by hand to expose the soil surface. The HydraProbe has four 50 mm prongs which were pressed into the soil by hand until no portion of the prongs were exposed. The Stevens HydraMon app (Stevens Water Monitoring Systems, Inc., Portland, OR, USA) was used to record data collected by the HydraProbe. At each soil moisture sampling location, three measurements were taken, approximately 300 mm apart, to generate an average soil moisture at each sampling location.

3.3.3 Soil Strength Measurement

Nine locations were pre-selected for testing based on varying topographic and soil texture conditions. The cone penetrometer was used at each location to estimate the depth of the critical layer for bevameter testing by pressing the cone tip into the soil at a rate of 30.5 mm/second. The critical layer was selected as the depth at which the cone penetrometer displayed soil strength greater than 1379 kPa which typically occurred within the first 30 mm to 80 mm of soil (Figure 3.4). At each testing site, surficial vegetation was removed from the testing area using electric gardening shears (Figure 3.5). After removal of surface vegetation, surficial soil was removed to the depth of the critical layer (estimated using the cone penetrometer) using a flat shovel and leveled (Figure 3.6), making sure the cleared area was no less than 220 mm in diameter to accommodate for placement of external surcharge. Figures 3.7 and 3.8 show the placement of the 2 kPa internal and external surcharge on the soil followed by the shear annulus. Sandpaper (40

grit; Figure 3.9) was used as the shear interface for all tests and replaced as needed to ensure sandpaper was not used on two different soil types without being replaced. For each test, the bevameter legs were adjusted so the shear annulus was parallel to the soil surface. Dead weight was applied to the bevameter to achieve shear annulus normal stresses of 19.2 kPa, 38.6 kPa, and 58.7 kPa. Tests conducted at 38.6 kPa and 58.7 kPa required the bevameter legs be staked into the soil to ensure the bevameter frame did not move during testing. Torque measured by the bevameter was recorded on a laptop computer (Figure 3.10). The torque sensor and data acquisition system used for field testing are described in Chapter 2. Each test was conducted for 60 seconds, rotating the shear annulus at a rate of 1 rpm. After the shear annulus was rotated 360 degrees, the test was terminated and the bevameter was relocated to the next prepared testing location. Figure 3.11 shows the soil surface at location SS-2 after termination of the bevameter test under a normal stress of 38.6 kPa. At each testing location, the bevameter test was conducted under each of the three normal stresses listed previously to fit a Mohr-Coulomb failure envelope to the data using the method of least squares linear regression, described in Chapter 2.

4. Results and Discussion

Soil strength patterns from the STRESS model and soil moisture patterns from the EMT+VS model were prepared for one soil strength sampling date (May 29, 2020). The testing region had an average soil moisture, $\bar{\theta} = 0.096$ ($m^3/m^{3)}$ which was used for input into the EMT+VS model. As discussed in Pauly (2019), dryer dates ($\bar{\theta}$ near 0.06) show little spatial variation in moisture patterns. Figure 3.12 displays the predicted soil moisture patterns produced by the EMT+VS model. Comparison of the predicted soil moisture from EMT+VS to measured soil moisture at each of the 21 sites produced a RMSE of 0.015 with moisture contents ranging from 0.080 to 0.140. The RMSE from the tested date is lower than the typical error of a TDR device

(Bogena et al., 2007) suggesting low predictive error of the EMT+VS model. Soil moisture measurements for the top 50 mm of soil were used for modeled strength estimates; however, future studies should consider measuring soil moisture at the critical depth for a more accurate measurement of bevameter strength sampling soil moisture.

Soil moisture estimations using the EMT+VS model in Pauly (2019) produced a RMSE value of 0.017 for a dry date with a spatial average soil moisture of $\bar{\theta}$=0.063. A moderate/wet sampling date produced a RMSE of 0.035 with a spatial average soil moisture of $\bar{\theta}$=0.192 and a wet sampling date produced a RMSE of 0.038 with an average soil moisture of $\bar{\theta}$=0.264. The predictive performance of the EMT+VS model in this study ($\bar{\theta}$=0.096) showed the lowest value of RMSE (0.015) compared to iterations of predicted soil moisture done in Pauly (2019). The model appears to produce lower RMSE values when conducted on dates with lower spatial average soil moisture based on the date tested in this study and the three dates tested in Pauly (2019).

Spatial prediction of ϕ at the field site is shown in Figure 3.13. Figure 3.14 displays the ϕ measured by the bevameter versus the ϕ predicted using class average values. Bevameter testing did not show peak shear strain behavior, therefore failure was defined at 60-degree angular displacement as discussed in Chapter 2. Friction angle predicted by the STRESS model ranged from 28 to 31 degrees (estimated using traditional geotechnical testing methods) while the measured ϕ ranged from 28 to 42 degrees. The resulting ϕ measured at location SS-1 (Table 3.1) has been flagged as a testing error as the ϕ of 59 degrees is too high to be viewed as reasonable, and therefore, was not included in the calculation of average values or RMSE. The high ϕ is likely to have been caused by the presence of dense roots or rocks at the testing location. The ϕ estimated by STRESS consistently underestimated values by 10 to 15 degrees resulting in a RMSE of 9 degrees.

The ϕ values measured from a drier date ($\bar{\theta}$=0.063) in Pauly (2019) resulted in measured ϕ ranging from 34 to 41 degrees with an RMSE of 8 degrees. For a moderate/wet ($\bar{\theta}$=0.19) date and wet ($\bar{\theta}$=0.264) date, measured ϕ ranged from 36 to 47 degrees and 29 to 49 degrees respectively. Because ϕ is based on class average values for each soil texture in the STRESS model, ϕ ranged for 28 to 31 degrees for all dates. As illustrated in Figure 3.14, ϕ was typically underestimated up to 20 degrees for all dates tested.

The underprediction of ϕ by the STRESS model may be caused by factors not included in the model which may lead to errors in the predicted values. The STRESS model predicts mineral soil strength and does not account for other factors which may contribute to the field strength of soil. The soils at the Drake Farm field site have the potential for calcium carbonate to act as a weak binding agent between soil particles (Erskine et al., 2017). Additionally, the presence of roots, and other organic matter below the soil surface are likely to increase ϕ but are not accounted for in the model.

Figure 3.15 displays the predicted c_θ at the field site for the date tested and a comparison of measured versus predicted c_θ is shown in Figure 3.16. Average c_θ measured using the revised bevameter procedure were lower than the predicted values at each of the nine sites tested. Predicted values of c_θ ranged from 7 kPa to 95 kPa while the measured values of c_θ ranged from 0 kPa to 12 kPa. When comparing the predicted c_θ versus measured c_θ, the resulting RMSE was 76.8 kPa. A dry sampling date in Pauly (2019) ($\bar{\theta}$=0.063) produced a RMSE value of 110 kPa with measured and predicted c_θ ranging from 0 kPa to 2.5 kPa and 12.5 kPa to 189 kPa respectively. A moderate/wet ($\bar{\theta}$=0.192) and a wet ($\bar{\theta}$=0.264) date produced RMSE values of 18.8 kPa and 9.1 kPa respectively, with measured c_θ ranging from approximately 0 kPa to 9 kPa and predicted c_θ

ranging from 1 kPa to 48 kPa for both dates. The STRESS model shows greater predictive performance for c_θ on wetter dates based on the four dates presented above. A full outline of the STRESS model performance on these dates ($\bar{\theta}$=0.063, 0.192, 0.264) can be found in Pauly (2019).

Parameters measured using the revised bevameter procedure agree with the parameters measured by Pauly (2019) based on RSME values. Using a revised bevameter procedure, measured parameters did not show improved RSME when compared to the predicted parameters from the STRESS model. The revised bevameter procedure is shown to reduce slip sinkage in a SM, increasing ϕ from 23 degrees (measured by grousers with no surcharge) to 34 degrees while c_θ remained relatively unchanged (5.9 kPa to 2.5 kPa respectively). While the revised bevameter procedure was developed to reduce the effects of slip sinkage in low strength, cohesionless soils, the soils at Drake Farm attain sufficient strength that slip sinkage is not considered to significantly impact parameter measurement when testing because these soils have a higher resistance to the mass flow of particles out from under the shear annulus. Removing the soil (typical 10-20 mm) to the critical layer and testing with sandpaper did not yield a significant difference when compared to the results from Pauly (2019). However, pressing grousers 16 mm into the soil before testing is hypothesized to have resulted in shearing at the same zone identified as critical for mobility by CI.

As shown in Figure 3.17, the STRESS model consistently overpredicts shear stress at Drake Farm up to 80 kPa for the three bevameter normal stresses tested in this study ($\bar{\theta} = 0.096$). Similarly, as shown in Figure 3.18, predicted shear strength on drier dates demonstrate overprediction of shear strength compared to wetter dates. This over-prediction of shear strength is hypothesized to result from an over-prediction of moisture-variable cohesion. Additional research into the origin of this over-estimation is needed. An additional factor that could help explain the discrepancies between measured and predicted values is the non-linearity of the failure

envelope observed in bevameter testing (see Chapter 2). Although failure envelopes produced over the stress range of 19.2 kPa to 58.7 kPa in the soils present at Drake Farm did not show apparent non-linearity soil strength data, further studies are required to observe the behavior of the failure envelope at higher normal stresses.

5. Summary and Conclusion

A revised bevameter procedure was tested at a field site in Northeastern Colorado. Shear strength was measured using a bevameter at nine sites. Each site was tested under three different normal stresses to measure ϕ and c_θ using the Mohr-Coulomb failure criteria. Bevameter testing was conducted using a coarse grit sandpaper as the shear interface. A 2 kPa surcharge internal and external to the shear annulus was applied to the soil surface for all tests. A cone penetrometer was used to determine the critical layer for testing at each of the nine testing locations. Surficial soil was removed down to the critical layer for bevameter testing. Soil moisture was measured at 21 locations using an in-situ soil moisture sensor and used for input into the EMT+VS model to predict downscaled soil moisture patterns. Downscaled soil moisture and interpolated soil data were used as input into the STRESS model. For the date tested, the following conclusions can be made:

1. Parameters measured using a revised field bevameter testing procedure did not show improved agreement to values predicted using the STRESS model compared to previous studied conducted by Pauly (2019). The consistent shear strength parameters produced by bevameter testing in this study and Pauly (2019) is hypothesized to be explained by the similarities between soil shearing by sandpaper at the critical layer and the shearing of grousers (which extend 16 mm into the soil) at the surface. Additionally, the soils tested at Drake Farm are not highly susceptible to the effects of slip sinkage under dry to moderate soil moisture conditions,

making the benefits of the revised bevameter procedure unpronounced for the conditions tested at this site.

2. Additional data are required to better understand the non-linearity of the failure envelope at normal stresses above 58.7 kPa at the Drake Farm site.
3. The STRESS model tends to underestimate ϕ and overestimate c_θ. Predictive error is introduced in modeling through the re-classification of soil types from USDA to USCS and the use of binned parameters generated for non-terramechanics focused applications. The results of this study illustrate the need to develop surficial-soil specific pedotransfer functions for use in the STRESS model and not rely on geotechnical class average soil strength parameters.
4. Continuous predictive relationships should be developed through an extensive soil strength data collection campaign using the revised bevameter procedure to relate surficial shear strength parameters to soil texture for improvement of STRESS model predictions.

6. Tables and Figures

Table 3.1. Measured θ, ϕ, and c_θ at the Drake Farm field testing site.

Location	Measured Moisture Content, θ	Measured Friction Angle, ϕ (degrees)	Measured Cohesion, c (kPa)
SS-1	0.10	59	0.0
SS-2	0.10	40	2.5
SS-3	0.10	41	0.0
SS-4	0.08	-	-
SS-5	0.08	-	-
SS-6	0.09	-	-
SS-7	0.09	-	-
SS-8	0.10	-	-
SS-9	0.08	-	-
SS-10	0.09	-	-
SS-11	0.08	-	-
SS-12	0.08	-	-
SS-13	0.08	-	-
SS-14	0.09	-	-
SS-15	0.09	-	-
SS-16	0.10	38	0.0
SS-17	0.09	29	12.1
SS-18	0.09	35	2.1
SS-19	0.13	33	5.1
SS-20	0.12	38	0.9
SS-21	0.14	42	1.5

- = measurement not taken

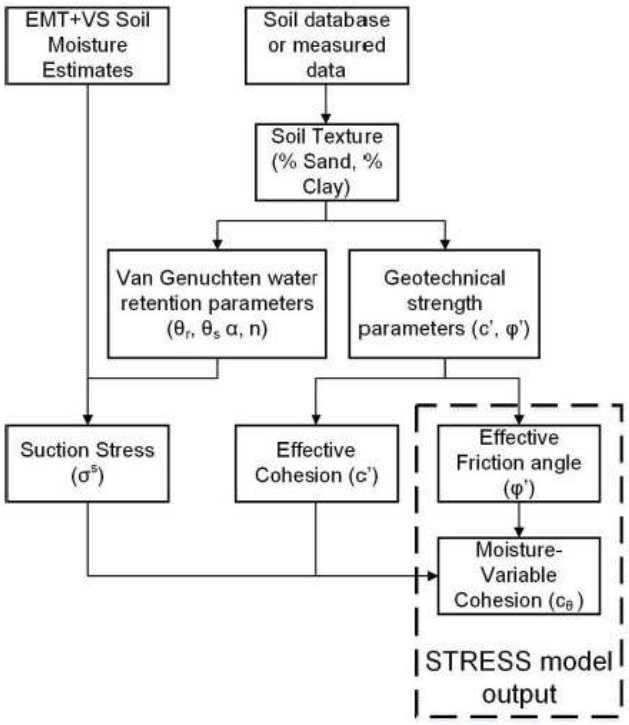

Figure 3.1. Diagram of stress model framework (Pauly, 2019).

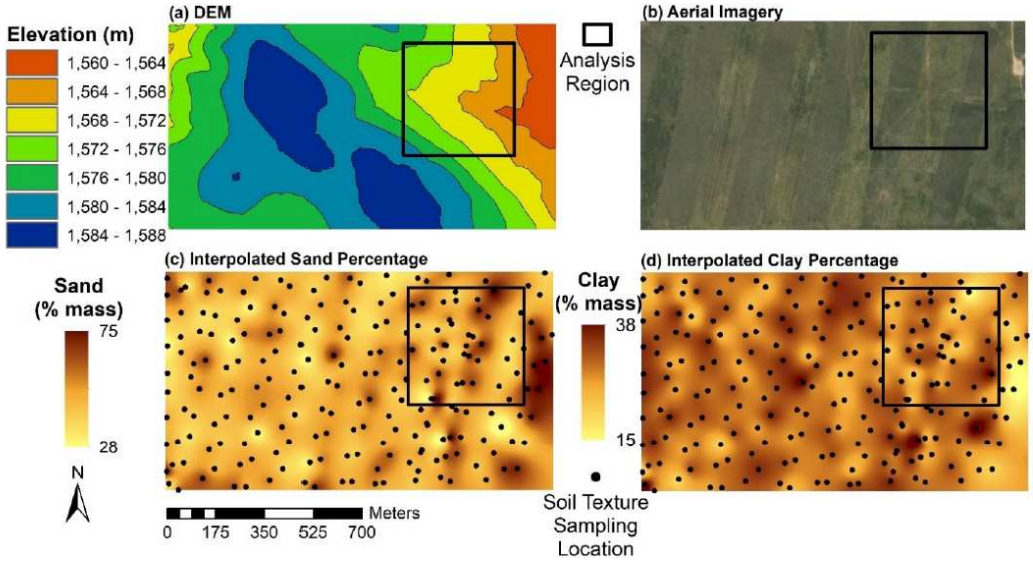

Figure 3.2. Drake Farm field site description with region of interest of this study shown by a black rectangle in each image including (a) digital elevation map (DEM), (b) aerial photograph, (c) interpolated percentage of sand by mass with 215 soil sampling locations, (d) interpolated percentage of clay by mass with 215 soil sampling locations (McCutcheon et al., 2006; Pauly et al., 2020).

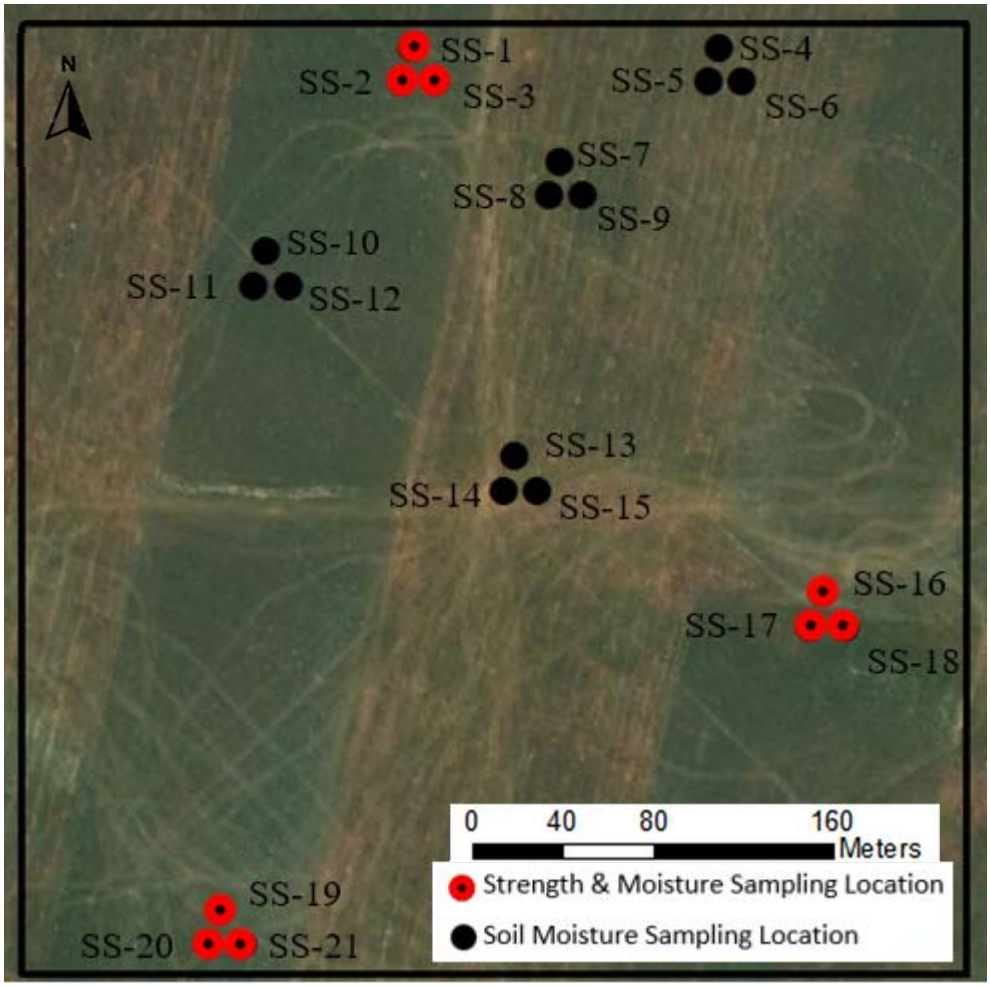

Figure 3.3. Soil strength and soil moisture sampling locations in the area of interest (approximately 400 m by 400 m) at the Drake Farm field site.

Figure 3.4. Pressing of cone penetrometer into the soil.

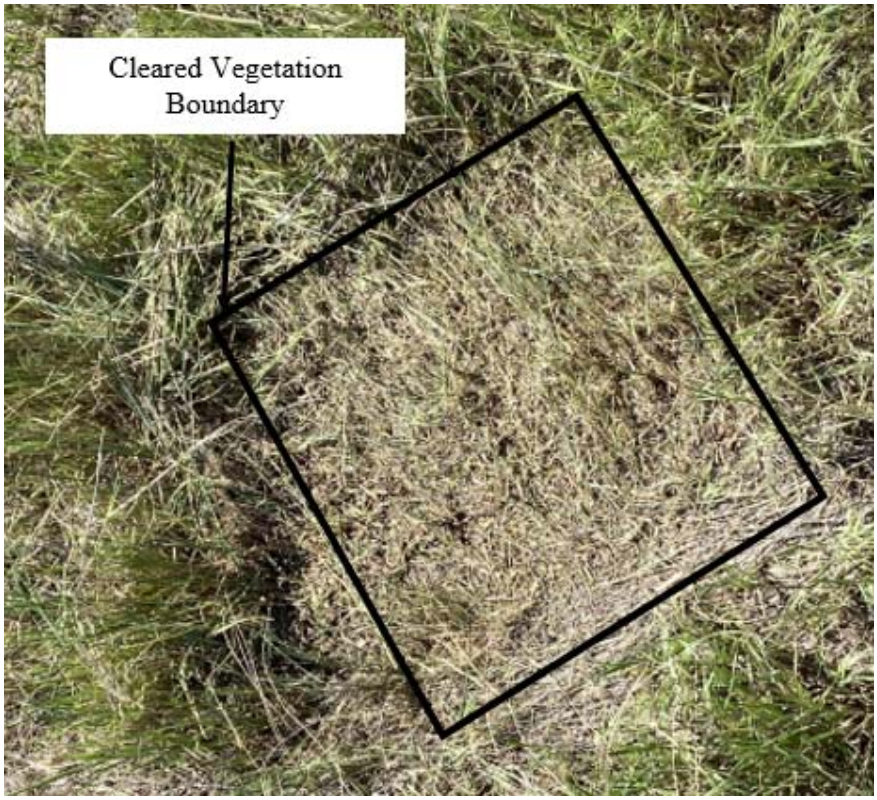

Figure 3.5. Soil strength testing location after vegetation has been cleared with an electric gardening shears.

Figure 3.6. Testing location after surficial soil has been removed.

Figure 3.7. Placement of internal and external surcharge on cleared soil surface.

Figure 3.8. Placement of shear annulus on the soil surface with internal and external surcharge.

Figure 3.9. Sandpaper as the shear interface on the bottom of shear annulus.

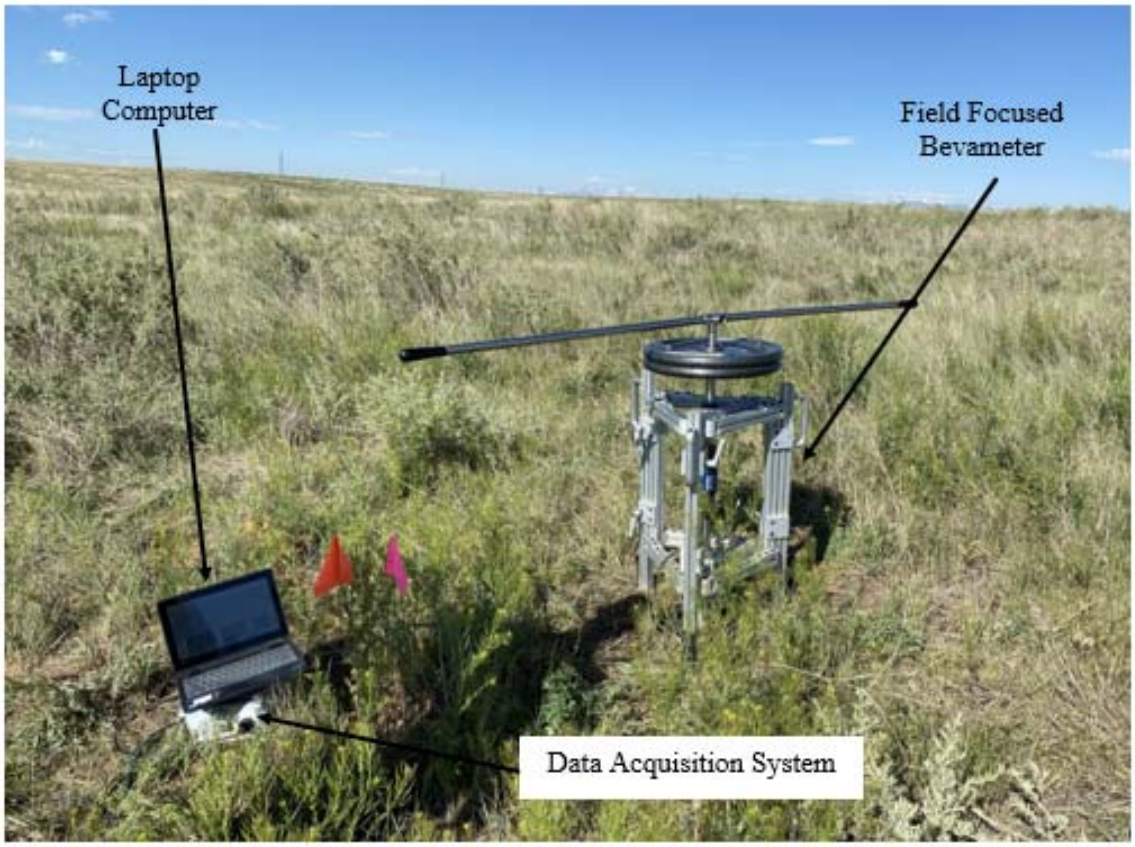

Figure 3.10. Field focused bevameter, laptop, and data acquisition system at the Drake Farm field testing site.

Figure 3.11. Soil surface after shearing by bevameter.

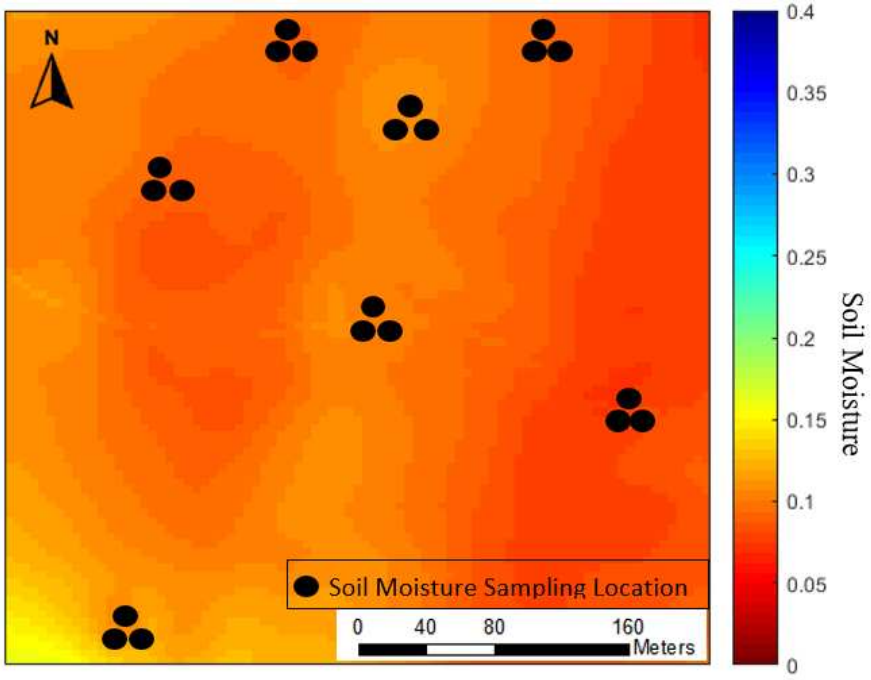

Figure 3.12. Downscaled soil moisture for the Drake Farm area of interest (approximately 400 m by 400 m) using the EMT+VS model with average soil moisture of 0.096.

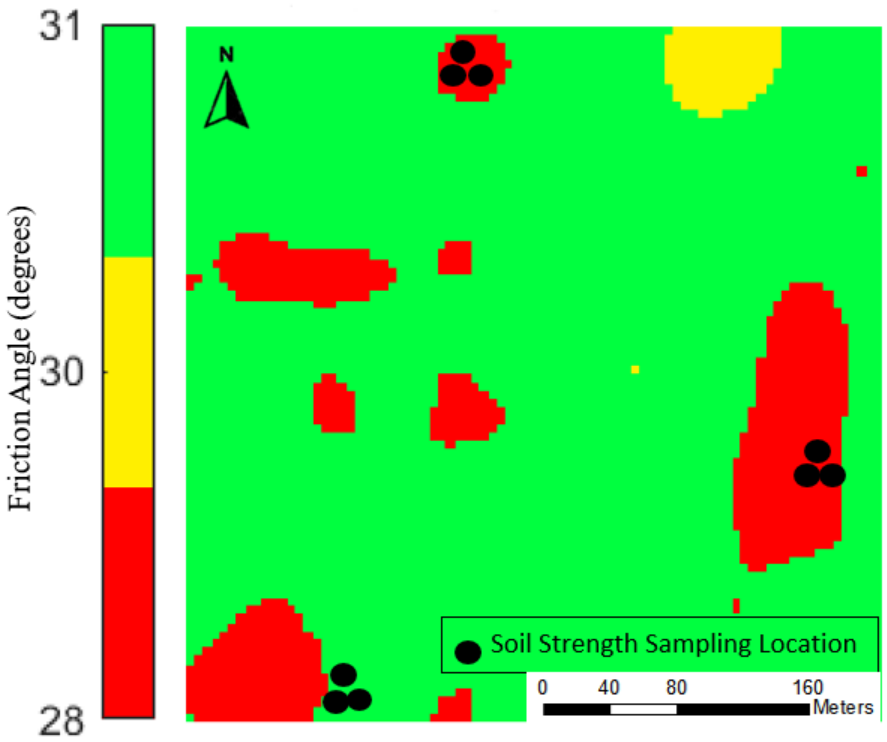

Figure 3.13. Friction angle estimates at the Drake Farm field site area of interest (approximately 400 m by 400 m) using the STRESS model.

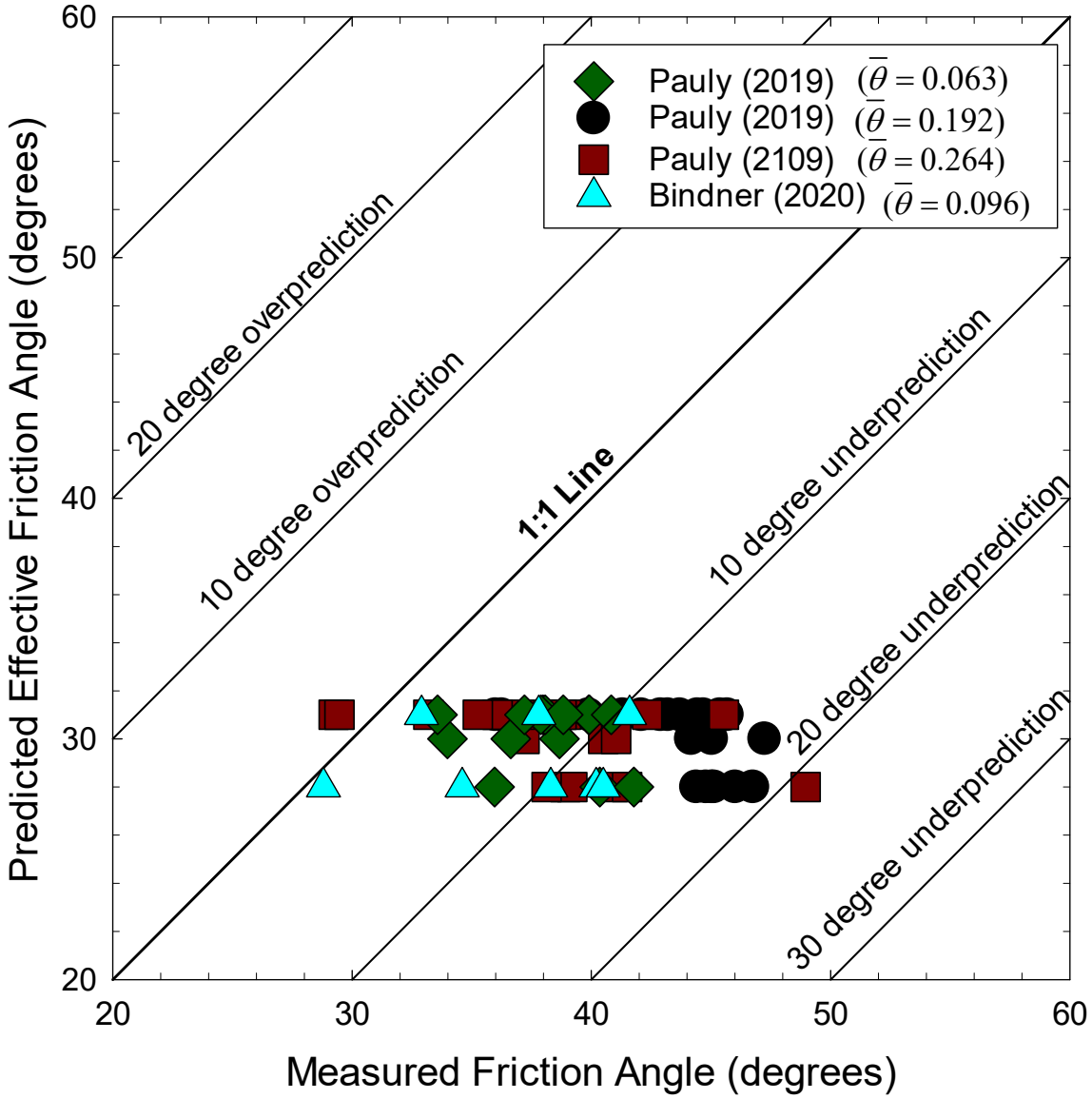

Figure 3.14. Comparison of measured to predicted ϕ vales at Drake Farm using the bevameter procedure described in Pauly (2019) at three different moisture contents and the method described in this paper (Bindner, 2020) for one moisture content.

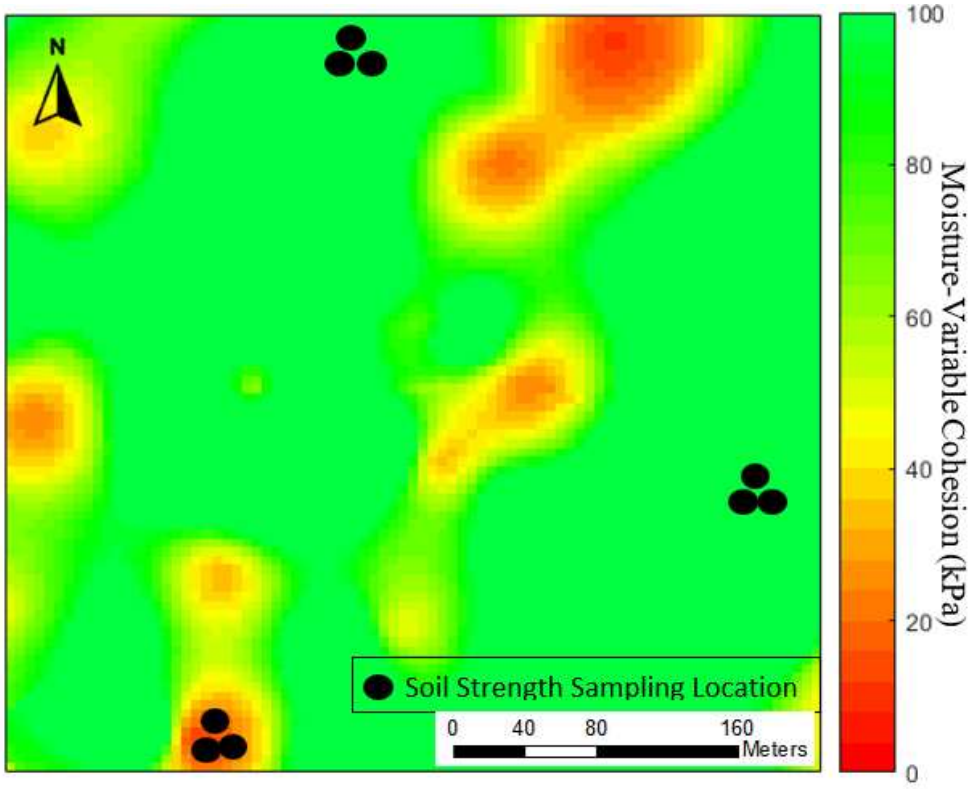

Figure 3.15. Moisture-variable cohesion at the Drake farm field site area of interest (approximately 400 m by 400 m) on a field testing day with an average soil moisture of 0.096.

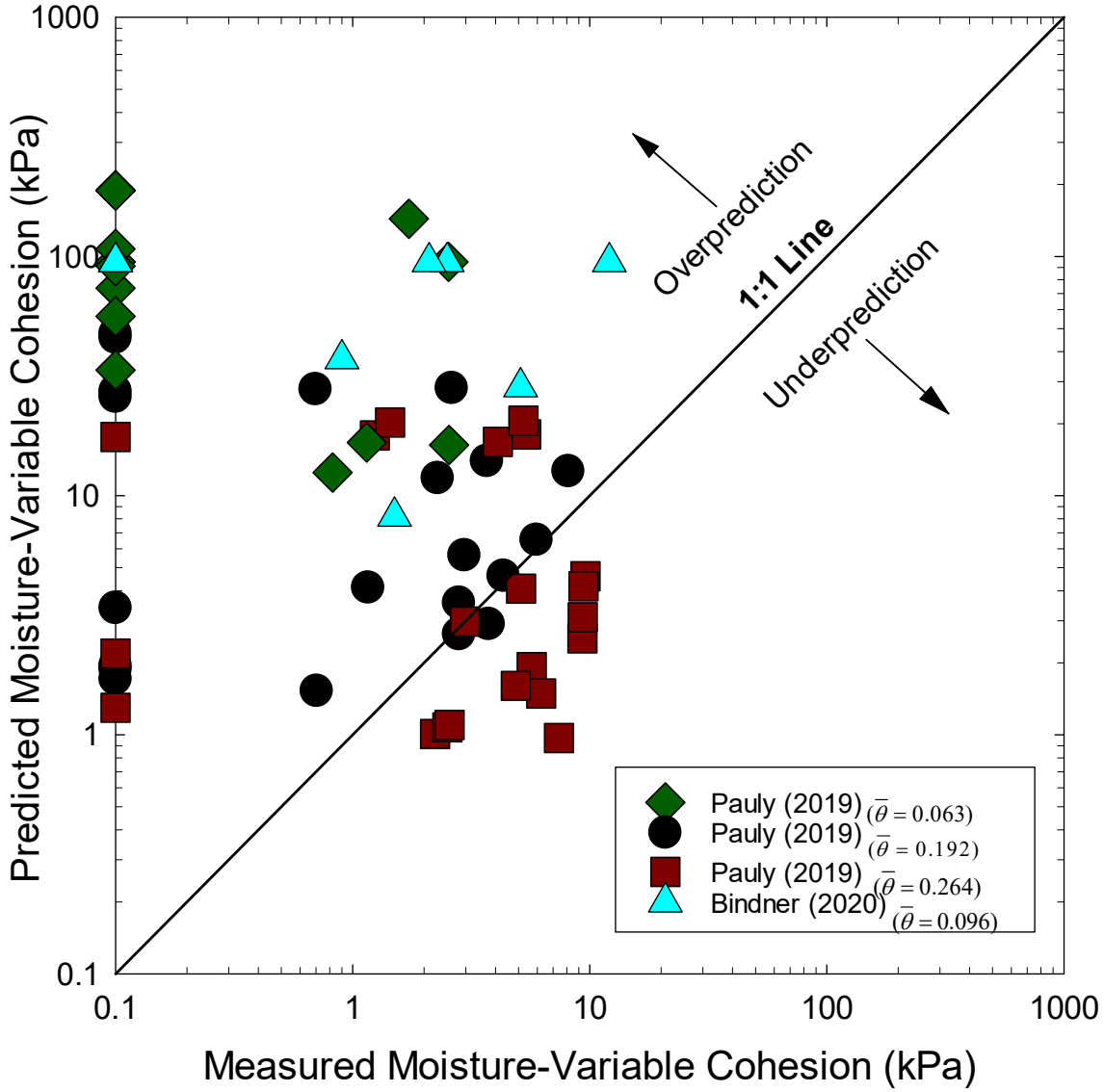

Figure 3.16. Comparison of measured to predicted c_θ values at Drake Farm using the bevameter procedure described in Pauly (2019) at three different moisture contents and the method described in this paper (Bindner, 2020) for one moisture content.

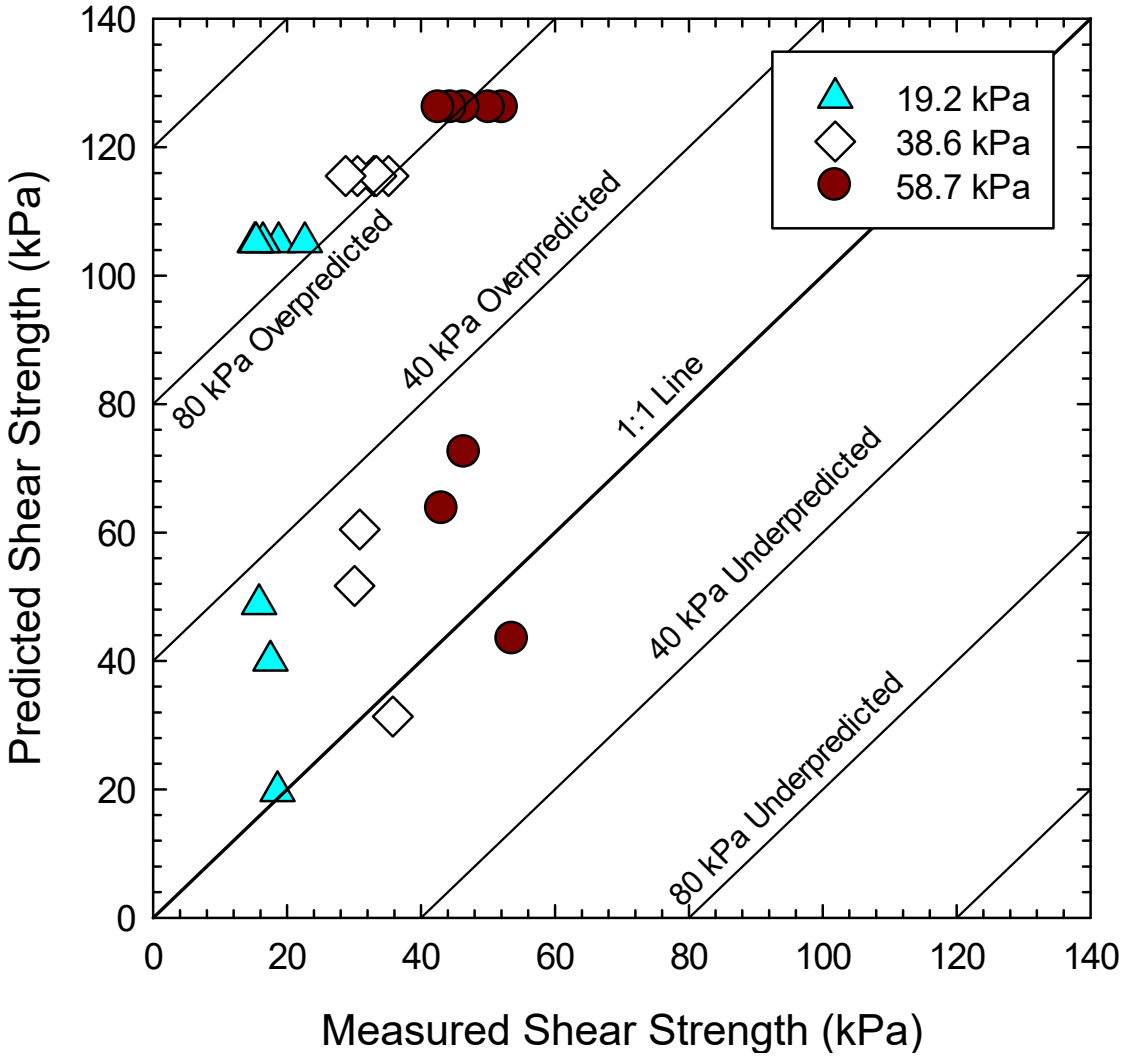

Figure 3.17. Comparison of measured to predicted shear stress for an average soil moisture of $\overline{\theta} = 0.096$ at the three bevameter normal stresses.

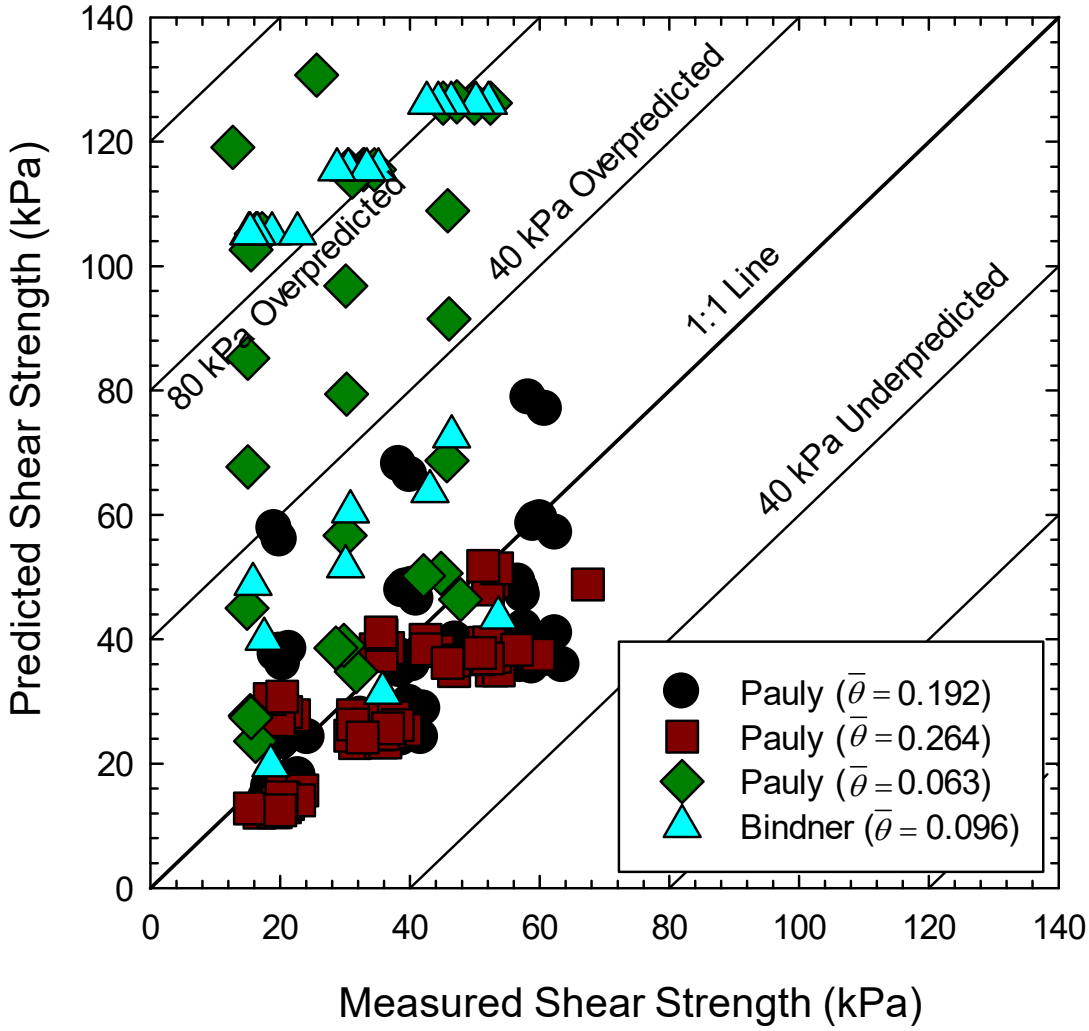

Figure 3.18. Comparison of measured to predicted shear stress for four moisture contents.

REFERENCES

ASTM D 3080/D 3080M-11. (2011). D3080/D3080M-11. Standard test method for direct shear test of soils under consolidated drained conditions. In *ASTM International* (Vol. 04, pp. 1–9). https://doi.org/10.1520/D3080

ASTM D1587. (2020). *Standard Practice for Thin-Walled Tube Sampling of Fine-Grained Soils for Geotechnical Purposes* (pp. 1–10). https://doi.org/10.1520/D1587

ASTM D4767. (2020). American Society of Testing Materials D4767 - 11. *American Society for Testing and Materials*, 1–11. https://doi.org/10.1520/D4767-11.2

Balling, O., Bradbury, M., Bruce, J., Cammarere, M., Choi, K., Dasch, J., Foster, C., Funk, M., Gaul, N., Hodges, H., Jain, A., Jayakumar, P., McCollough, M., Niemann, J., Elham, R., Scalia, J., Wasfy, T., & Wojtysiak, B. (2019). *AVT-248 Next-Generation NATO Reference Mobility Model (NG-NRMM) Development*. https://doi.org/01/15/2020

Bekker, M. G. (1956). *Theory of Land Locomotion: The Mechanics of Vehicle Mobility*. University of Michigan Press.

Bekker, M. G. (1962). *Mechanics of Off-The-Road Locomotion*. 25–44.

Bekker, M. G. (1969). *Introduction to Terrain-Vehicle Systems*. University of Michigan Press.

Bishop, A. W., & Blight, G. E. (1963). Some Aspects of Effecive Stres in Saturated and Partly Saturated Soils. *Geotechnique*, *13*(3), 177–197. https://doi.org/05/11/2020

Bogena, H. R., Huisman, J. A., Oberdörster, C., & Vereecken, H. (2007). Evaluation of a low-cost soil water content sensor for wireless network applications. *Journal of Hydrology*, *344*(1–2), 32–42. https://doi.org/10.1016/j.jhydrol.2007.06.032

Bowles, J. E. (1992). *Engineering Properties of Soils and Their Measurement* (4th ed.). Irwin/McGraw-Hill.

Bradbury, M., Dasch, J., Gonzalez, R., Henry Hodges, S., Jain, A., McCullough, M., Jody Priddy, U., Wojtysiak, B., Wong, J., Jayakumar, P., Hoenlinger, M., & Wegmann GmbH, K.-M. (2016). *Next-Generation NATO Reference Mobility Model (NG-NRMM) Final Report by NATO Exploratory Team ET-148 Authors ET-148 Leaders*. https://apps.dtic.mil/dtic/tr/fulltext/u2/1011267.pdf

Choi, K. K., Jayakumar, P., Funk, M., Gaul, N., & Wasfy, T. M. (2019). Framework of Reliability-Based Stochastic Mobility Map for Next Generation NATO Reference Mobility Model. *Journal of Computational and Nonlinear Dynamics*, *14*(2), 1–10. https://doi.org/10.1115/1.4041350

Edwards, M. B., Dewoolkar, M. M., Huston, D. R., & Creager, C. (2017). Bevameter testing on simulant Fillite for planetary rover mobility applications. *Journal of Terramechanics*, *70*, 13–26. https://doi.org/10.1016/j.jterra.2016.10.004

Erskine, R. H., Sherrod, L. A., & Green, T. R. (2017). Measuring and Mapping Patterns of Soil Erosion and Deposition Related to Soil Carbonate Concentrations Under Agricultural Management. *Journal of Visualized Experiments*, *2017*(127). https://doi.org/10.3791/56064

Fredlund, D. G., Morgenstern, N. R., & Widger, R. A. (1978). Canadian Geotechnical Revue canadienne. *Canadian Geotechnical Journal*, *15*, 313–321.

García-Gaines, R. A., & Frankenstein, S. (2015). USCS and the USDA Soil Classification System, Development of a Mapping Scheme. *UPRM and ERDC Educational and Research Internship Program*, *March*, 37. https://apps.dtic.mil/dtic/tr/fulltext/u2/a614144.pdf

Green, T. R., Erskine, R. H., Murphy, M. R., Ma, L., Ascough, J. C., McMaster, G. S., Dunn, G. H., & Ahuja, L. R. (2009). Space-time dynamics of soil water and process interactions in semi-arid terrain, Colorado, USA. *18th World IMACS Congress and MODSIM09*

International Congress on Modelling and Simulation: Interfacing Modelling and Simulation with Mathematical and Computational Sciences, Proceedings, *July*, 1851–1857.

Green, Timothy R., & Erskine, R. H. (2011). Measurement and inference of profile soil-water dynamics at different hillslope positions in a semiarid agricultural watershed. *Water Resources Research*, *47*(12), 1–16. https://doi.org/10.1029/2010WR010074

Humboldt. (2011). *Corps of Engineers Cone Penetrometer*. https://www.humboldtmfg.com/corps-of-engineers-cone-penetrometer.html

Janosi, E. J.; Karafiath, L. L. (1981). Improved Technique of Field Ring Shear. *Proceedings of the International Conference/International Society for Terrain Vehicle Systems*.

Lambe, T. William; Whitman, R. V. (1969). *Soil Mechanics*. Wiley.

Lessem, A., Mason, G., & Ahlvin, R. (1996). Stochastic vehicle mobility forecasts using the NATO reference mobility model. In *Journal of Terramechanics* (Vol. 33, Issue 6, pp. 273–280). https://doi.org/10.1016/S0022-4898(97)00010-4

Liston, R. A. (1973). *Combined normal and tangential loading of soil*. Michigan Technological University.

Lu, N., Godt, J. W., & Wu, D. T. (2010). A closed-form equation for effective stress in unsaturated soil. *Water Resources Research*, *46*(5), 1–14. https://doi.org/10.1029/2009wr008646

Lu, N., & Likos, W. J. (2004). *Unsaturated Soil Mechanics*. John Wiley & Sons, Inc.

Mason, G. L., Salmon, J. E., McLeod, S., Jayakumar, P., Cole, M. P., & Smith, W. (2019). An overview of methods to convert cone index to bevameter parameters. *Journal of Terramechanics*, *87*, 1–9. https://doi.org/10.1016/j.jterra.2019.10.001

Moreland, S., Skonieczny, K., Wettergreen, D., Creager, C., & Asnani, V. (2011). Soil motion

analysis system for examining wheel-soil shearing. *17th International Conference of the International Society for Terrain Vehicle Systems 2011, ISTVS 2011*, 49–56.

Nowatzki, E. A., & Karafiath, L. L. (1974). General Yield Conditions in a Plasticity Analysis of Soil-Wheel Interaction. *Journal of Terramechanics*, *11*(1).

Okello, A. (1991). A review of soil strength measurement techniques for prediction of terrain vehicle performance. *Journal of Agricultural Engineering Research*, *50*(C), 129–155. https://doi.org/10.1016/S0021-8634(05)80010-1

Oravec, H. A. (2009). *Understanding mechanical behavior of lunar soils for the study of vehicle mobility*. 662.

Osman, M. S. (1964). The measurement of soil shear strength. *Journal of Terramechanics*, *1*(3), 54–60. https://doi.org/10.1016/0022-4898(64)90039-4

Pauly, M. J. (2019). *Modeling and Field Evaluation of Unsaturated Soil Strength for Vehicle Mobility* [Colorado State University]. https://mountainscholar.org/handle

Payne, P. C. (1956). The Relationship Between the Mechanical Performance of Simple Cultivation Implements. *Journal of Agrucultural Engineering Research*.

Ranney, K. J., Niemann, J. D., Lehman, B. M., Green, T. R., & Jones, A. S. (2015). A method to downscale soil moisture to fine resolutions using topographic, vegetation, and soil data. *Advances in Water Resources*, *76*, 81–96. https://doi.org/10.1016/j.advwatres.2014.12.003

Reece, A. R. (1964). *Problems of Soil Vehicle Mechanics*.

Schaap, M. G., Leij, F. J., & Van Genuchten, M. T. (2001). Rosetta: A computer program for estimating soil hydraulic parameters with hierarchical pedotransfer functions. *Journal of Hydrology*, *251*(3–4), 163–176. https://doi.org/10.1016/S0022-1694(01)00466-8

Senatore, C., & Iagnemma, K. D. (2011). Direct shear behaviour of dry, granular soils for low

normal stress with application to lightweight robotic vehicle modelling. *17th International Conference of the International Society for Terrain Vehicle Systems 2011, ISTVS 2011*, 1–11.

Shoop, S. A. (1993). *Terrain Characterization for Trafficability*. 23.

Skempton, A. W. (1954). The pore-pressure coefficients a and b. *Geotechnique*, *4*(4), 143–147. https://doi.org/10.1680/geot.1954.4.4.143

Staff, S. S. (2018). *Soil Survey Geographic (SSURGO) Database for Weld County, CO*. USDA-NRCS. https://websoilsurvey.sc.egov.usda.gov

Stevens, M. T., Towne, B. W., Mason, G. L., Priddy, J. D., Osorio, J. E., & Barela, C. A. (2013). *Procedures for One-Pass Vehicle Cone Index (VCI 1) Determination for Acquisition Support*. *August*.

van Genuchten, M. T. (1980). A Closed-form Equation for Predicting the Hydraulic Conductivity of Unsaturated Soils. *Soil Science Society of America Journal*, *44*(5), 892–898. https://doi.org/10.2136/sssaj1980.03615995004400050002x

Williams, J., Mason, G., Vahedifard, F., & Borazjani, A. (2017). *Expansion and Application of Database Records for Off-road Vehicle Expansion and Application of Database Records for Off-road Vehicle Environments (DROVE)*. *May*.

Wong, J. Y. (2001). *Theory of Ground Vehicles* (Third Edit). John Wiley & Sons, Inc.

APPENDIX A

This appendix contains AutoCAD design drawings for a field-focused pressure-sinkage device for measurement of Bekker-Wong pressure sinkage parameters. A comprehensive parts list can be found in Table 2.1. Pressure is provided by a trailer jack which is advanced at a constant rate. The vertical driving force is to be provided by a user rotating the crank at a constant rate to advance plates of different diameter into the soil. Figure A.1 through A.4 show the dimensions and layout of the field focused pressure sinkage device. The pressure-sinkage design was created, but not constructed because soil strength parameters, and not pressure-sinkage relationships, were selected as the focus of this study.

Table A.1. Parts list for the field-focused pressure sinkage device.

Part Name	Quantity	Part Number	Vendor
Bolt-On Jack, top wind, 10" travel (2000 lb. capacity)	1	151443	Cequent Trailer
Trailer Jack Drop Leg	1	500377	AutoZone
Side-Mount Bearing, 4" Long, for 1" High Rail T-Slotted Framing (120 Lb capacity)	8	47065T783	McMaster-Carr
Hand Brake for 1" and 2" Wide Sleeve Bearing Carriage for T-Slotted Framing	8	60585K31	McMaster-Carr
Silver Corner Bracket, 2" Long for 1" High Rail T-Slotted Framing	42	47065T239	McMaster-Carr
Silver Diagonal Brace for 1" High Single Rail, 6" Long	12	47065T186	McMaster-Carr
Snap on End Cap for 1" High Single Rail T-Slotted Framing	10	47065T91	McMaster-Carr
Silver Tee Surface Bracket for 1" High Single Rail	12	47065T278	McMaster-Carr
L-Shaped Connector for 1" High Single Rail T-Slotted Framing	18	5537T315	McMaster-Carr
Mounting Foot	4	47065T841	McMaster-Carr
Silver Straight Surface Bracket	8	47065T255	McMaster-Carr
T-Slotted Framing Single Rail, Silver, 1" High x 1" Wide, Solid (10 ft.)	5	47065T101	McMaster-Carr
T-Slotted Framing Single Rail, Silver, 1" High x 1" Wide, Solid (8 ft.)	1	47065T101	McMaster-Carr
T-Slotted Framing Single Rail, Silver, 1" High x 1" Wide, Solid (6 ft.)	1	47065T101	McMaster-Carr
SSM or SSM 2 Sealed S-Type Load Cell Load Cell (1000 lb. capacity)	1	SSM 2 Sealed S-Type Load Cell	Interface, Inc.
LVDT	1	TBD	Omega Engineering Inc.
Transducer Amplifier	1	TBD	-

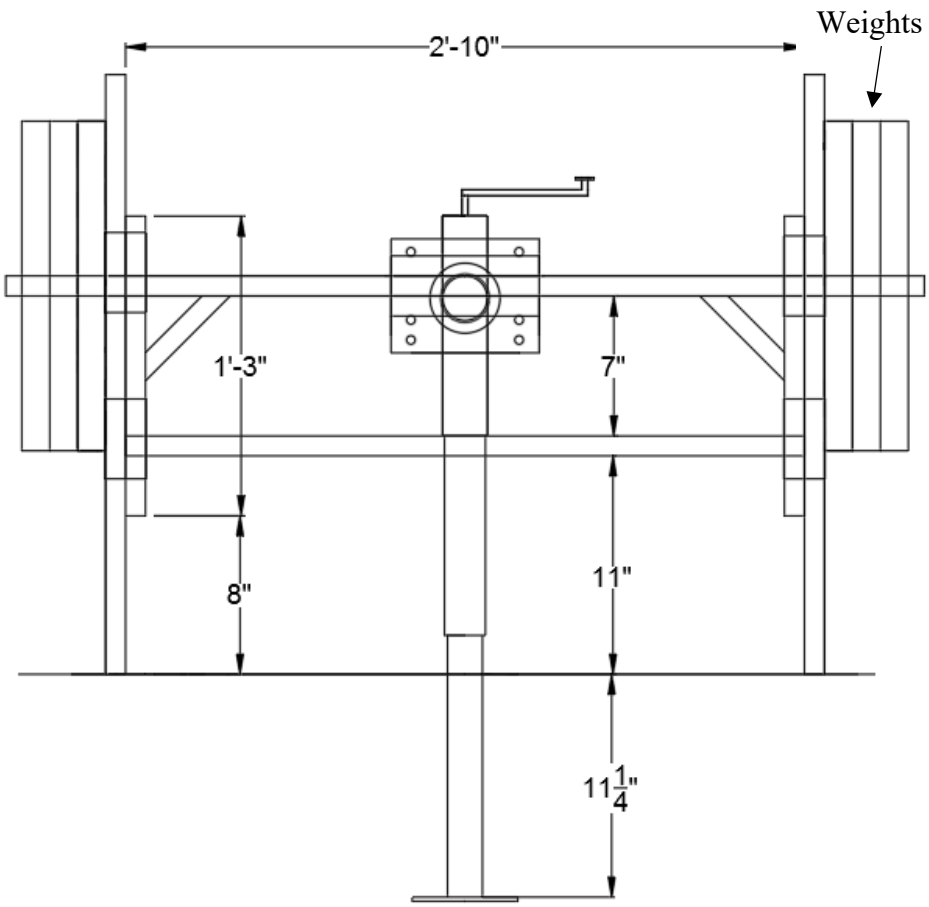

Figure A.1. Section view of the field-focused pressure sinkage device in the fully extended position.

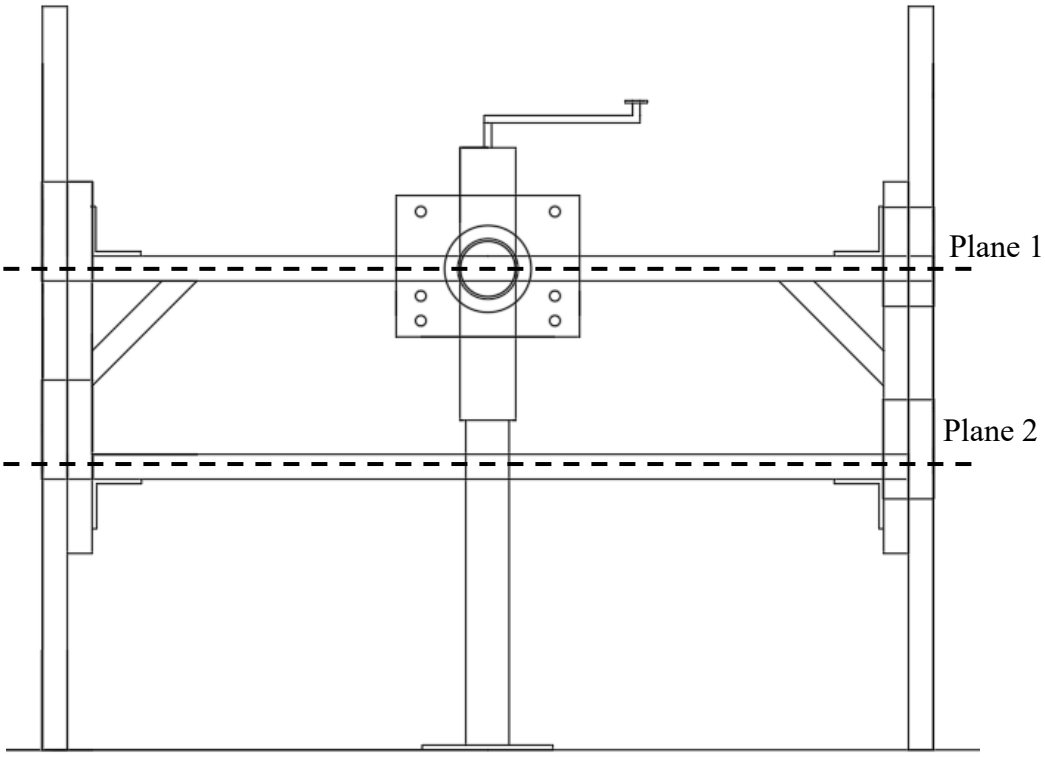

Figure A.2. Section view of the field-focused pressure sinkage device in the fully retracted position.

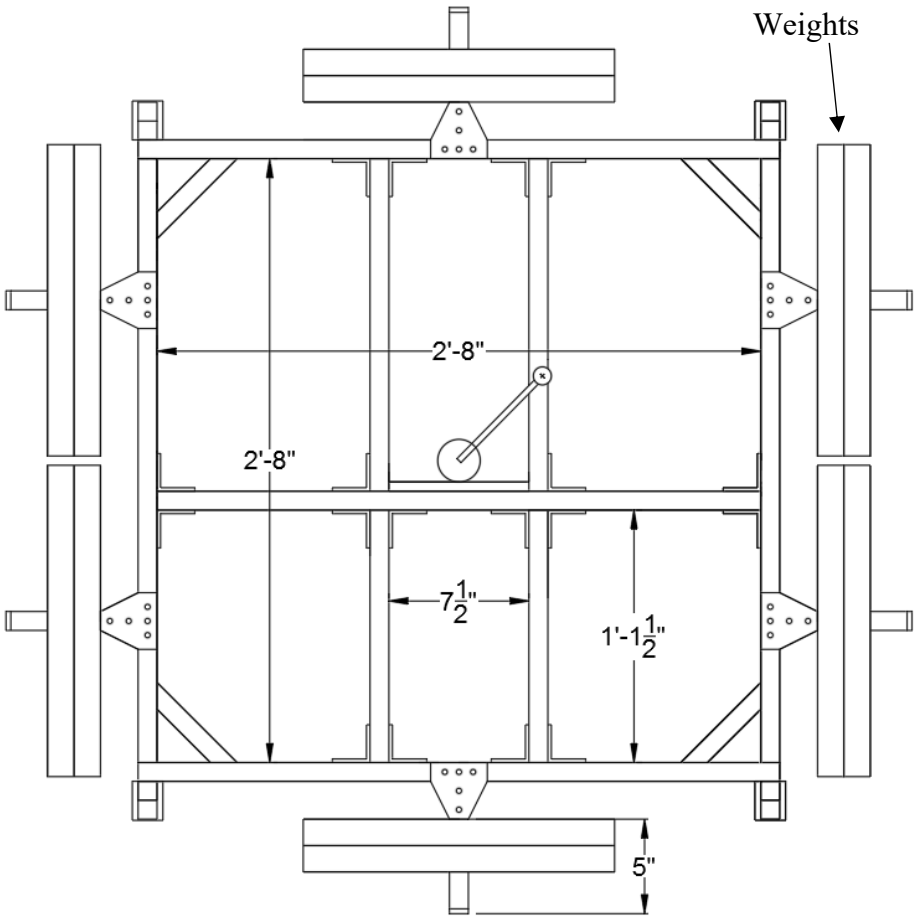

Figure A.3. Plan view of the machine for Plane 1 shown in Figure A.2.

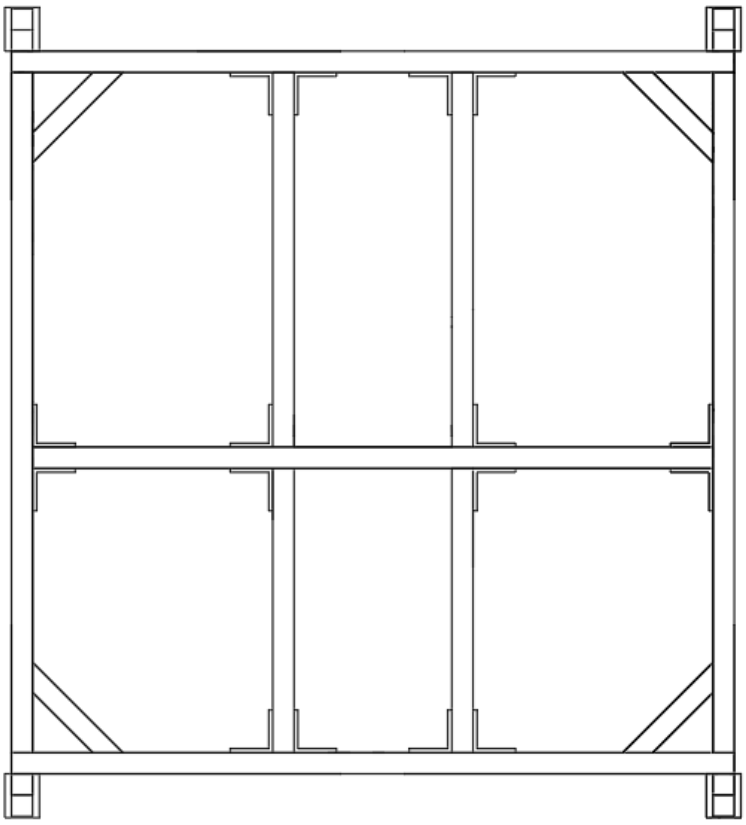

Figure A.4. Plan view of the machine for Plane 2 shown in Figure A.2.

APPENDIX B

B.1 Scope

Consolidated undrained triaxial testing was conducted to evaluate the feasibility for measurement of field collected unsaturated surficial soil strength. This appendix explains the field sampling and triaxial testing procedures for soil collected from a field-testing site in northeastern Colorado (Drake Farm).

B.2 Background

Triaxial testing of soil is used to determine shear strength parameters under controlled drainage conditions. A typical triaxial set up is shown in Figure 2.7. Cylindrical specimens can be prepared in a laboratory or collected as intact field samples. Specimens are encased in an impermeable latex membrane with a porous stone on either side to promote drainage, followed by end platens. The specimen is placed in a pressure cell and tubes attached to the end platens are connected to a pressure panel. The pressure cell is then inundated with water. Specimen pressure, referred to as back pressure, and cell pressure are controlled by a pressure panel as shown in Figure 2.7. Saturated testing conducted to measure total and effective shear strength parameters must be near saturation to minimize error. To achieve near saturation in the soil, saturation is developed in two phases: initial saturation and backpressure saturation. During initial saturation, de-aired water is allowed to flow through the soil, displacing air in the void space with water. However, after initial saturation, some air remains. To remove the remaining air, backpressure saturation is used. Pockets of air remaining in the soil void space are dissolved by incrementally increasing backpressure. To verify sufficient saturation, Skempton's pore pressure coefficient, *B*, is measured

(Skempton, 1954). The specimen is considered to be sufficiently saturated when *B* is greater than or equal to 95% (ASTM D4767, 2020). For saturated testing, consolidation is begun after the saturation phase. The consolidation phase is begun immediately after sample preparation for unsaturated triaxial testing.

The desired consolidation stress is achieved by incrementally increasing cell water pressure while allowing water or air within the specimen to drain for saturated and unsaturated testing, respectively. Cell pressure is increased until the desired effective stress is achieved. The soil is then placed in the shearing apparatus. Specimen drainage conditions are set and a strain rate appropriate for the application is selected. Pressure transducers record changes in porewater pressure thought the test (for saturated testing only) and axial load is measured by a load cell.

B.3 Methods and Materials

B.3.1 Drake Farm Soil

Figure B.1 displays three sampling locations selected from the Drake Farm field site. The three sampling locations were chosen for expected varying soil conditions. The soil collected from these sites were used to conduct unsaturated and saturated triaxial testing and soil classification. Soils were collected on two dates, Day One represented dry soil conditions (average saturation of 14%) and Day Two represented moist soil conditions (average saturation of 29%). The soils were classified by conducting, specific gravity, hydrometer analysis, and sieve analysis. Results of these tests are summarized in Table B.1.

B.3.2 Sample Collection

Samples were collected in 50 mm diameter brass thin-walled sampling tubes with a length of 100 mm. Vegetation was cleared from the surface of the soil using electric gardening shears (Figure B.2). The brass tubes were advanced into the soil at a constant rate of 10 mm/second. Once the top of the sampling tube was level with the ground surface, the soil around the tube was removed and the sampling tube was extracted and sealed to maintain in-situ moisture conditions. This process is shown in Figures B.3 and B.4.

B.3.3 Unsaturated Consolidated Undrained Triaxial Testing

Before testing the samples for soil strength, samples were carefully prepared for triaxial testing taking care to minimize sample disturbance. First, the caps on either end of the brass sampling tubes were removed and samples were placed into a hydraulic jack soil extruder. The soil was extruded 6 mm and the exposed dry and loose soil was trimmed as shown in Figure B.5. The sample was then fully extruded. A 0.3 mm thick latex membrane of 50 mm diameter was placed around the extruded sample. Filter paper followed by a circular porous plastic disk was placed on either end of the specimen and encased by the latex membrane. O-rings were then placed around the latex membrane on the end platens to prevent leakage of cell water into the specimen (Figure B.6).

A pressure cell was placed around the fully prepared sample and filled with water. Cell pressure was brought to 4.8 kPa, then increased by a factor of two until the desired stress of 13.8 kPa, 27.6 kPa, or 41.4 kPa was achieved. Pore air pressure was allowed to dissipate through hoses connected to the specimen during the consolidation phase. Pore air pressure dissipation was assumed to occur nearly instantly based on observed specimen volumetric compression, therefore, the cell pressure was increased immediately after the prior pressure increase. Once the desired cell

pressure was achieved, the triaxial cell was moved to the shearing piston (Figure 2.7). A pressure transducer was connected to the specimen boundary and all other drainage lines were closed. All specimens were sheared at a rate of 50.8 mm/minute (approximately 50% strain/minute) to simulate bevameter shearing rates (to the extent possible) while not exceeding the device limitations. A LVDT recorded displacement and a load cell recorded force developed in the shearing piston. All samples were sheared to an axial displacement of 20 mm (approximately 20% strain).

For each set of three tests conducted at different confining pressures, Mohr Circles were plotted using:

$$\sigma_1 = \sigma_d + \sigma_3$$
$$\sigma_3 = \sigma_c$$

where σ_1 is the major principal stress, σ_d is the maximum deviator stress, σ_3 is the minor principal stress and σ_c is the confining stress. For each set of three Mohr circles, a linear Mohr-Coulomb failure envelope was fit.

B.3.4 Saturated Consolidated Undrained Triaxial Testing

The sample preparation procedure described in Section B.3.3 of this appendix was followed for saturated triaxial testing. Once specimens were prepared and placed in the pressure cell, the ASTM standard procedure was followed for testing cohesive soils in a consolidated undrained triaxial compression test (ASTM D4767, 2020). Specimens were consolidated to 13.8 kPa, 27.6 kPa, or 41.4 kPa before shearing. Shearing was conducted at a strain rate of 1% strain/hour (approximately 1 mm/ hour) to a total of 20% strain (approximately 20 mm).

B.4 Results and Discussion

Figures B.8 through B.10 display the linear Mohr-Coulomb failure envelopes for three test sites on two different dates. Tables B.2 and B.3 display the saturation conditions of the soils tested. Testing of these soils generated variable ϕ with changing moisture conditions. Because ϕ is a material property, ϕ is expected to remain constant for duplicate specimens with the same composition and density, regardless of moisture conditions. Cohesion is expected to vary with moisture. However, for unsaturated triaxial testing *c* remained relatively constant regardless of changing moisture conditions. Variations in ϕ in unsaturated triaxial tests are hypothesized to result from various degrees of sample disturbance during sampling, transport, and test setup associated with different unsaturated conditions in different specimens, and heterogeneity in the soil tested.

The unsaturated triaxial testing of unsaturated specimens demonstrated significant limitations. Samples disturbance is difficult to avoid during field sampling, especially without heavy machinery which is required to follow standard field sampling procedures (ASTM D1587, 2020). For samples with low levels of saturation, the soil did not have sufficient cohesive strength to resist crumbling during the process of extruding and sample preparation. Figure B.11 illustrates the soil moisture profile for samples collected on Day 1. The low moisture contents near the soil surface made preparation impractical for the first 6 mm of soil (Figure B.7). The remaining soil required light compaction to avoid sample crumbling during preparation, further changing the specimen relative to the in-situ condition.

The triaxial test yields valuable results for traditional geotechnical applications. However, testing is time consuming, expensive, and complicated. The inability to test soils in-situ is one of the biggest disadvantages to the test. Arguments have been made that triaxial testing does not

closely enough represent vehicle stress conditions for accurate determination of vehicle soil strength properties even under ideal testing conditions (see Chapter 2, Results and Discussion). Additionally, for most studies, the triaxial test is not practical given typical schedule and budget constraints. For these reasons, triaxial testing on unsaturated samples collected in-situ is not recommended for the measurement of shear strength parameters representative of near-surface terramechanics applications.

B.5 Tables and Figure

Table B.1. Soil properties for the three soils collected from the Drake Farm field sampling location.

Soil Property	ASTM Method	SS-7	SS-17	SS-20
USDA Classification	N/A	Sandy Loam	Sandy Loam	Loam
Specific Gravity, G_s	D 854 - 14	2.65	2.63	2.65

Table B.2. Shear strength parameters for two sampling dates at three locations along with specimen saturation and specimen dry density.

Test	Average Saturation, S (%)	Average Dry Density (g/cm^3)	Friction Angle, ϕ' (degrees)	Cohesion c (kPa)
Day 1_SS-7	16%	1.3	22	38
Day 2_SS-7	25%	1.3	27	21
Day 1_SS-17	13%	1.4	38	25
Day 2_SS-17	16%	1.3	31	24
Day 1_SS-20	13%	1.4	39	21
Day 2_SS-20	47%	1.5	33	18

Table B.3. Effective shear strength parameters for three saturated specimens sampled from three site locations.

Test	Average Saturation, S (%)	Effective Friction Angle ϕ' (degrees)	Effective Cohesion c' (kPa)
D2_SS-7	100%	44	1
D2_SS-17	100%	29	6
D2_SS-20	100%	21	4

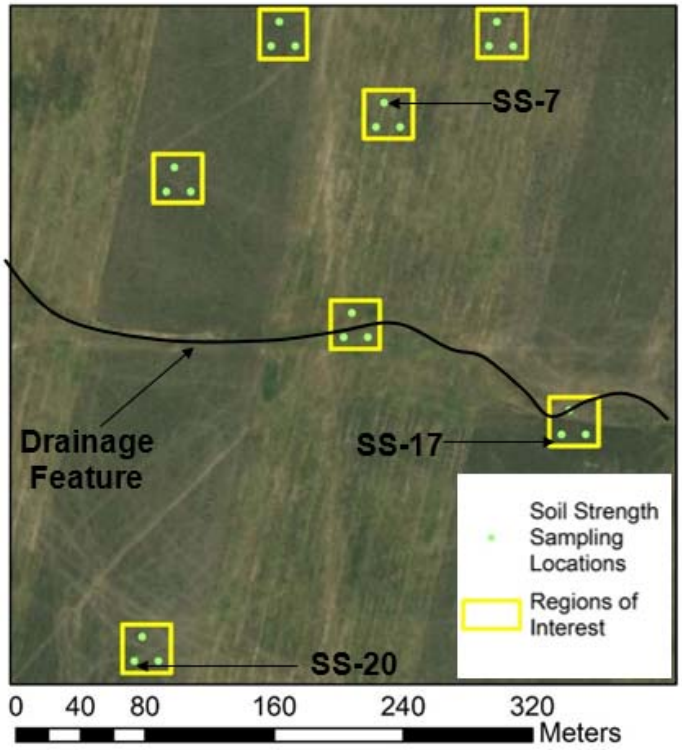

Figure B.1. Aerial image of the Drake Farm field testing site including labels of the three sampling locations for unsaturated consolidated undrained triaxial testing (Pauly, 2019).

Figure B.2. Electric gardening shears used for removal of surface vegetation before soil sampling.

Figure B.3. Drake Farm soil sampling procedure including (a) pressing of brass sampling tube into soil (b) sampling tube advanced completely into the soil (c) removal of soil around brass sampling tube (d) soil after removal of brass sampling tube.

Figure B.4. Sample collected from Drake Farm sealed in a brass sampling tube to preserve in-situ moisture conditions.

Figure B.5. Latex membrane placed around the sample preparation mold after removal of top 6 mm of soil just before sample is extruded into the membrane.

Figure B.6. Soil sample in latex membrane with O-rings placed around the end platens on either end of the specimen to prevent leakage of water into or out of the specimen.

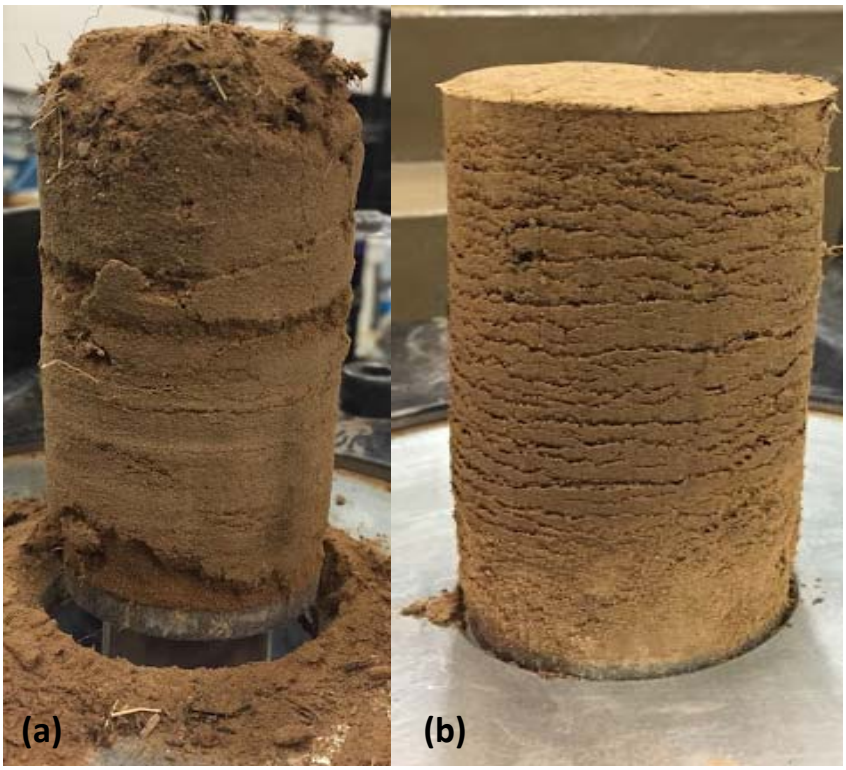

Figure B.7. Extruded soil sample collected on (a) a dry date and (b) a wet date.

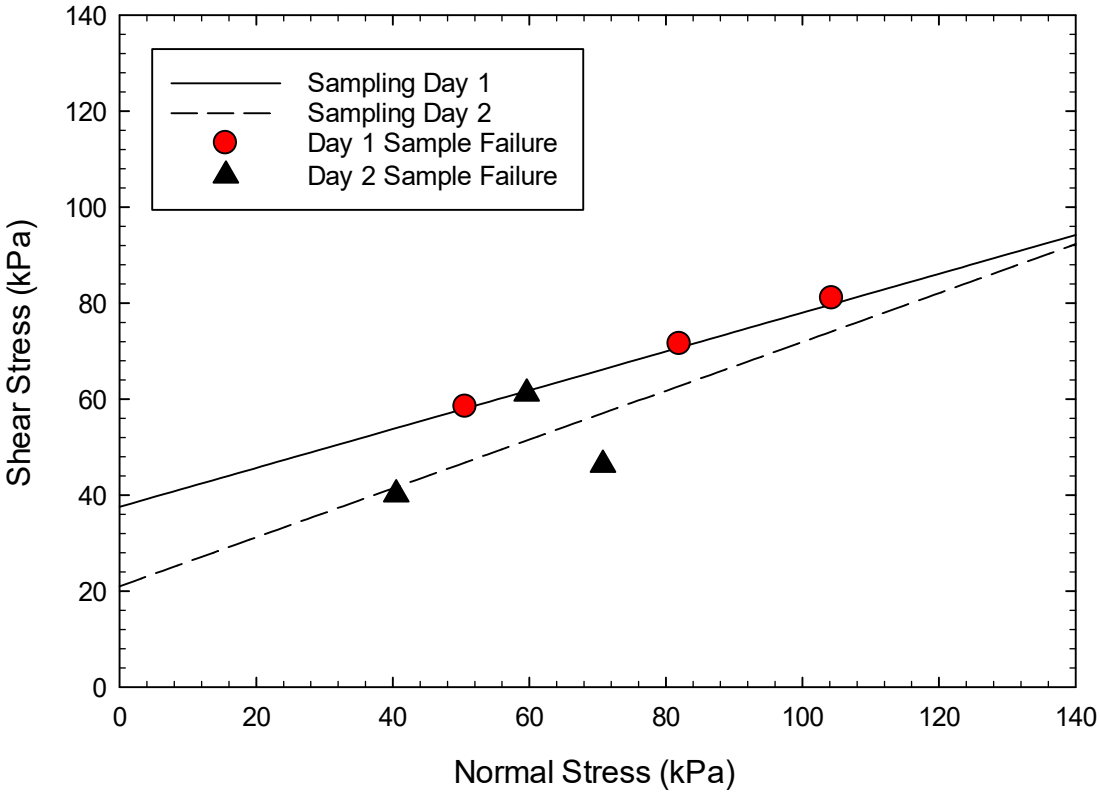

Figure B.8. Total stress data and Mohr-Coulomb failure envelopes for two sampling dates at the Drake Farm field testing site (Location: SS-7).

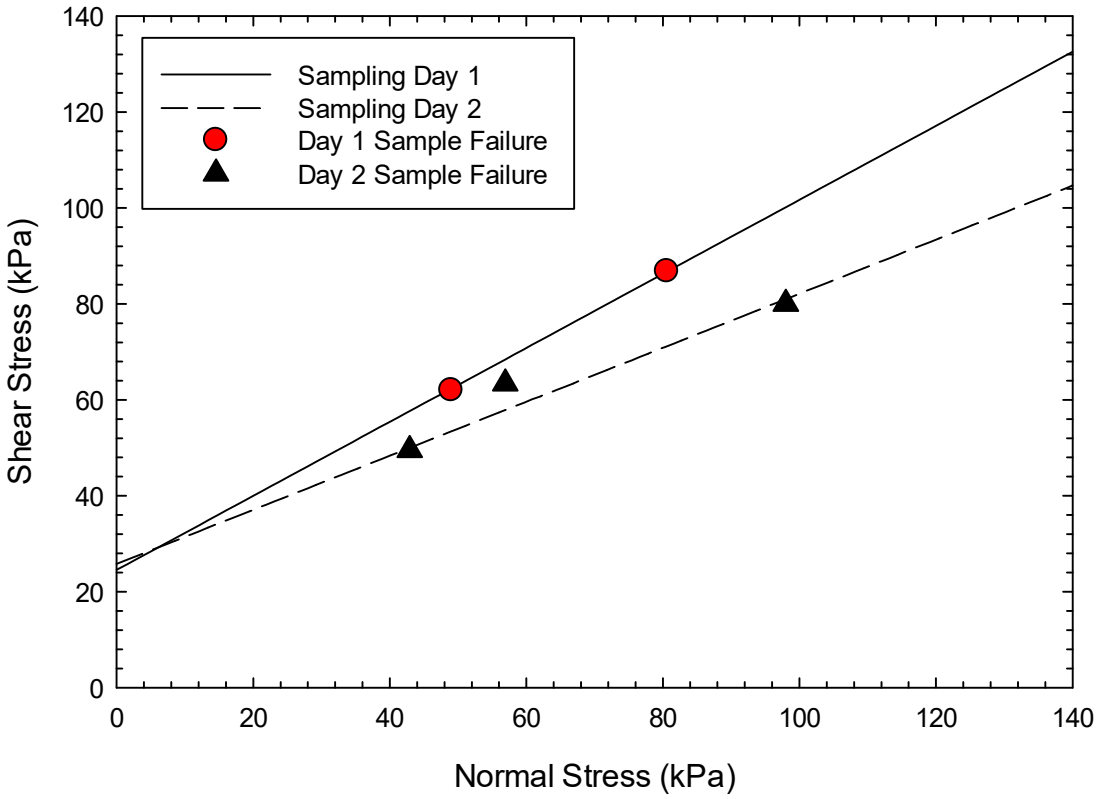

Figure B.9. Total stress data and Mohr-Coulomb failure envelopes for two sampling dates at the Drake Farm field testing site (Location: SS-17); Day 1 sample tested under 4.8 kPa normal stress was omitted from data due to a breach in latex membrane during testing due to a small stick in the soil profile.

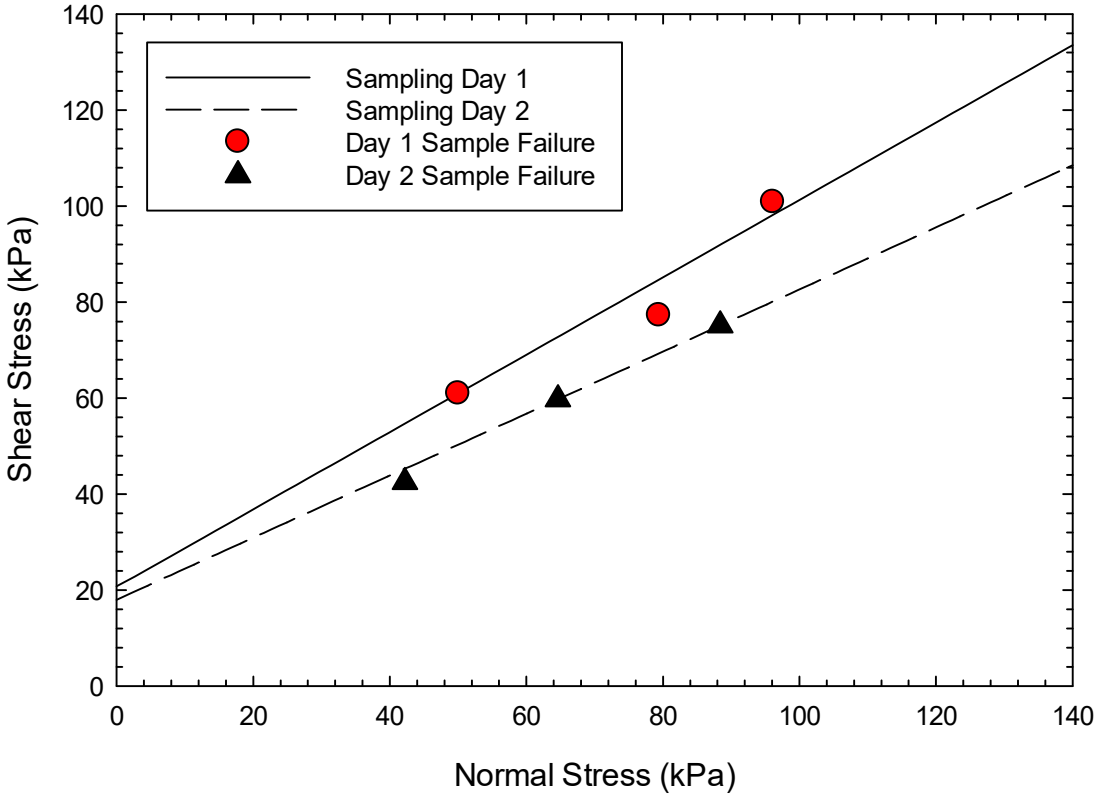

Figure B.10. Total stress data and Mohr-Coulomb failure envelopes for two sampling dates at the Drake Farm field testing site (Location: SS-20).

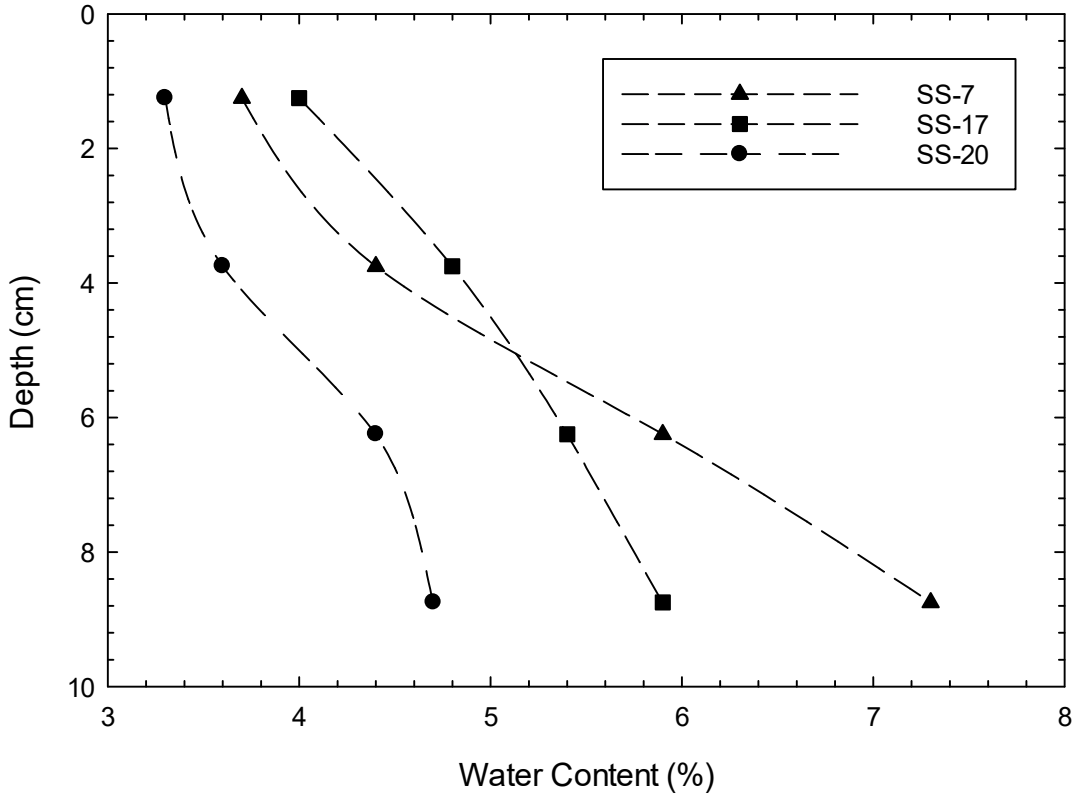

Figure B.11. Gravimetric water content profiles for samples collected at three sites at the Drake Farm field testing site.

APPENDIX C

C.1 Scope

A porewater pressure transducer was added to a bevameter shear annulus. The pressure transducer measured the development of porewater pressure at the shear annulus-soil interface. The sensor was calibrated and tested on a CH to observe the development of porewater pressure during annulus shearing.

C.2 Background

Understanding the drainage conditions for a soil is critical for soil strength analyses. Various shearing rates have been used in bevameter testing (Pauly, 2019). However, a more rapid shearing rate in a fine-grained soil could lead to the development of undrained conditions and excess porewater pressure. Equations C.1 and C.2 define the relationship between porewater pressure (u), total stress (σ), effective stress (σ'), effective shear strength parameters c' and ϕ', and shear strength (τ):

$$\sigma' = \sigma - u \tag{C.1}$$

$$\tau = c' + \sigma' \tan \phi' \tag{C.2}$$

Because shear strength is a function of effective stress, the development of excess porewater pressure in a soil decreases the effective stress on the soil and therefore decreases the soil shear strength. This concept is critical in terramechanics applications because soil pressures often develop rapidly when sheared by a vehicle. This could lead to the overestimation of soil strength in soils which behave undrained in terramechanics applications.

C.3 Methods and Materials

C.3.1 High Plasticity Clay

A high plasticity clay (USCS CH) was used for porewater pressure testing. A full description of this soil can be found in Chapter 2, Section 3.1. Relevant soil properties can be found in Table 2.1. The soil was prepared at 85% maximum dry density in a rectangular plastic container with dimensions 51 cm length by 38 cm width by 13 cm height. Water was then ponded to a depth of 5 cm atop the soil and the container was sealed for 72 hours to ensure near saturation of the soil (to the extent that would exist in the field). After 72 hours, the seal was removed, and the remaining ponded water was siphoned off.

C.3.2 Bevameter Procedure

Bevameter testing was conducted under an internal and external surcharge of 2 kPa. A coarse sandpaper (40 grit) was used as the shear interface. The soil was incrementally loaded at 100 second intervals. At time, t = 0 seconds, a normal stress of 19.2 kPa was applied to the shear annulus followed by 38.6 kPa and 58.7 kPa. At t = 300 seconds, the soil was sheared at a rate of 1 rpm for 30 seconds. After shearing, porewater pressure was observed until full dissipation of excess porewater pressure; testing was then terminated. Porewater pressure was measured by a 0-103.5 kPa Pressure Transducer (Omega Engineering Inc., Norwalk, CT) and data were recorded on a laptop computer (Figure C.1).

C.4 Results and Discussion

Figure C.3 illustrates the porewater pressure measurement at the shear interface during bevameter testing. Phase 1 represents the loading phase. While the development of porewater pressure was expected in Phase 1, the data indicates there was no development of excess porewater pressure. Shearing was initiated at the start of Phase 2. The soil exhibited undrained conditions during the shearing phase, as shown by the spike in porewater pressure to 3.5 kPa. Shearing was followed by dissipation of excess porewater pressure in Phase 3 after shearing was terminated. This study supports that fine-grained soils can develop excess porewater pressure at the shear interface in bevameter testing and that some portion of this excess pore water pressure can be measured with a porewater pressure transducer. However, additional research is needed to explore and quantify this important aspect of surficial soil shear behavior.

C.5 Tables and Figures

Figure C.1. Shear annulus with porewater pressure transducer.

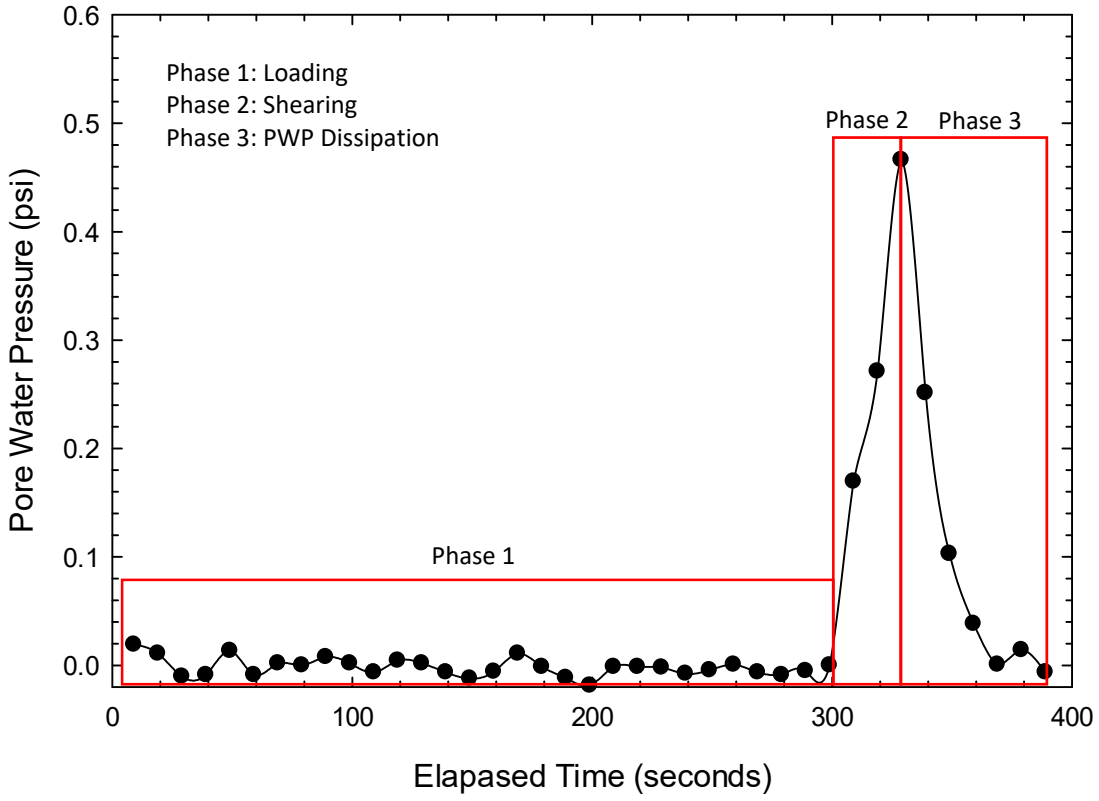

Figure C.2. Porewater pressure development in a bevameter test on a saturated CH under a normal stress of 58.6 kPa; Phase 1 represents loading of the shear annulus; Phase 2 represents rotation of the shear annulus; and Phase 3 represents the dissipation of excess porewater pressure after shearing.